

# Mechanisms rectifying the annual mean response of tropical Atlantic rainfall to precessional forcing

Michelle Tigchelaar<sup>1</sup>  · Axel Timmermann<sup>2</sup>

Received: 28 November 2014 / Accepted: 6 September 2015 / Published online: 19 September 2015  
© The Author(s) 2015. This article is published with open access at Springerlink.com

**Abstract** Numerous reconstructions of tropical hydroclimate in the Pleistocene display substantial variability on precessional timescales. Precessionally-induced insolation variations, with a mean period of  $\sim 21,000$  years, affect the strength of the seasonal cycle, but not annual mean insolation. The existence of variations in annual mean climate on precessional timescales therefore hints at the existence of nonlinear mechanisms that rectify the zero annual mean forcing into a non-zero annual mean response. The aim of this study is to identify these nonlinear rectification mechanisms. The traditional view of precessionally-forced precipitation changes is that tropical precipitation increases with summer insolation. By comparing two simulations with an earth system model (CESM1.0.3) we find that this paradigm is true for continental but not for oceanic changes in precipitation. Focusing on the Atlantic intertropical convergence zone (ITCZ), we find that the continental temperature and precipitation response to precessional forcing are key rectifiers of annual mean precipitation over the ocean. A boundary layer response to temperature changes over northern Africa affects the *meridional position* of the ITCZ over the North Atlantic in boreal spring and summer, but not in fall and winter. Over the equatorial and South Atlantic, the *intensity* of precipitation is strongly impacted by diabatic forcing from the continents through an adjustment of the full troposphere. Although the top of atmosphere insolation forcing is seasonally symmetric, continental

precipitation changes are largest in boreal summer, thus skewing the annual mean response. These results show that it is important to take into account the seasonality of climatic forcings, even when studying annual mean climate change.

**Keywords** Atlantic ITCZ · Tropical precipitation · Precession · Orbital forcing · Nonlinear rectification

## 1 Introduction

Out of Earth's three orbital parameters—eccentricity, obliquity, and precession—responsible for low-frequency climate variability (Milankovitch 1941), the one with the largest expression in the tropics is precession (Berger 1978; Laskar et al. 2004). With a period of  $\sim 21,000$  years (21 ka), the precessional cycle determines at what time of year the earth is closest to the sun. It thus changes the strength of the seasonal cycle in incoming solar radiation at each latitude, and it does so anti-symmetrically across the hemispheres: When the seasonal cycle is stronger in the Northern Hemisphere ('minimum precession', similar to e.g. 11 ka) it is weaker in the Southern Hemisphere, and vice versa ('maximum precession', similar to e.g. present-day). The strength of the precessional cycle is modulated by eccentricity, which describes how elliptical Earth's orbit is. When eccentricity is low—i.e. the orbit is close to circular—precession hardly influences seasonality.

Many tropical paleoclimate records display substantial precessional variability, much more so than polar records such as the EPICA and NGRIP ice cores (EPICA Community Members 2004; North Greenland Ice Core Project Members 2004). This recorded precessional variability can result from either a physical climate forcing, or from the

✉ Michelle Tigchelaar  
mtigch@hawaii.edu

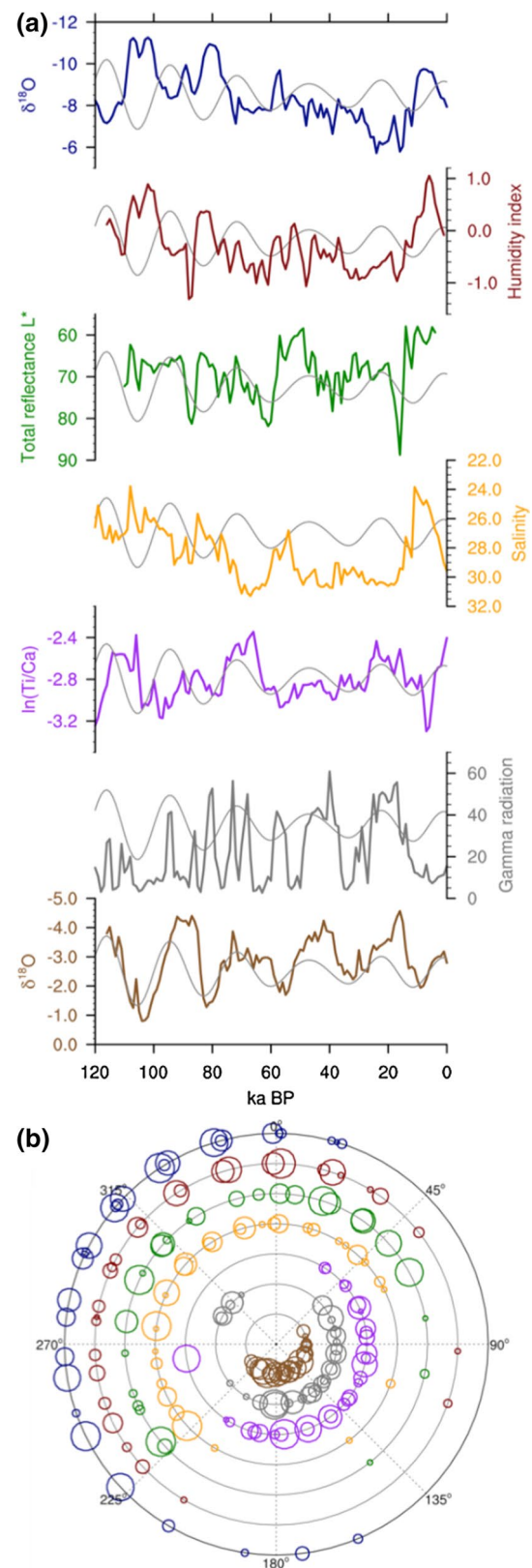
<sup>1</sup> Department of Oceanography, University of Hawaii at Manoa, Honolulu, HI, USA

<sup>2</sup> International Pacific Research Center, University of Hawaii at Manoa, Honolulu, HI, USA

**Fig. 1 a** Paleorecords of tropical hydroclimate against the precessional cycle ( $e \sin(\omega)$ , see Sect. 2; grey); from top to bottom: composite of speleothem  $\delta^{18}\text{O}$  from Chinese caves (25°–32°N): Dongge (Dykoski et al. 2005), Hulu (Wang et al. 2004), Sanbao (Wang et al. 2008); North African humidity index 20.8°N (Tjallingii et al. 2008); sediment total reflectance in Cariaco Basin 10.7°N (Deplazes et al. 2013); salinity reconstruction from Ba/Ca in Eastern Atlantic (2.5°N) (Weldeab et al. 2007);  $\ln(\text{Ti}/\text{Ca})$  from West Pacific Warm Pool (2.5°S) (Tachikawa et al. 2014); sediment gamma radiation from Bolivia (20.3°S) (Fritz et al. 2004); speleothem  $\delta^{18}\text{O}$  from Botuvera cave (Brazil; 27.2°S) (Wang et al. 2004, 2007; Cruz et al. 2005). Records are ordered from north to south, with inferred precipitation increasing along the y-axis; A 1000-year running mean was applied to each record. **b** Precessional phase  $\omega$  (see Sect. 2) of the 25 % highest values of the records in (a), scaled by amplitude. Colors correspond to the records of (a)

seasonal bias of climate recorders (Huybers and Wunsch 2003) as for instance shown for SST reconstructions and the production rates of coccolithophorids and planktonic foraminifera in Timmermann et al. (2014) and Antarctic temperatures and snow accumulation in Laepple et al. (2011). Figure 1a shows a compilation of various proxy reconstructions of tropical hydroclimate (smoothed with a 1000-year running mean) over the past 120 ka, contrasted against the precessional forcing. The records are ordered from North to South, with inferred precipitation increasing along the y-axis. All of these records contain some component of precessional variability, with maximum precipitation generally coinciding with maximum local summer insolation. Because precessional forcing of seasonal cycle strength is anti-phased between hemispheres, there is a North to South anti-symmetry in the timing of precipitation maxima. This is also illustrated in Fig. 1b, which for each record shows the precessional phase of the 25 % highest precipitation values, scaled by amplitude. Clearly the majority of the Northern Hemisphere precipitation maxima are associated with a precessional phase opposite to that of the Southern Hemisphere precipitation maxima.

The role of precession in driving tropical climate variability has been addressed in a number of modeling studies. Most notably Clement et al. (2004) showed that the (seasonal) response of tropical climate to precessional forcing can be as large as, and substantially different from, the response induced by the high-latitude climatic forcing usually thought to be the main driver of long-term climate variability. Many studies have particularly focused on the role of precession in driving changes in the South-East Asian and African summer monsoon systems (e.g. Kutzbach and Guetter 1986; Braconnot and Marti 2003; Tuenter et al. 2003; Wyrwoll et al. 2007; Kutzbach et al. 2008; Shi et al. 2011). In addition, there are numerous studies focusing on time slice experiments of Pleistocene climates that also involve precessional change, such as the mid-Holocene and the last interglacial (e.g. Kutzbach and Otto-Bliesner 1982;



Kutzbach and Liu 1997; Zhao et al. 2005; Braconnot et al. 2008; Khon et al. 2010, 2012; Bosmans et al. 2012). These studies emphasize the importance of differential heating of

land and ocean in driving seasonal precipitation changes in the continental monsoon regions.

Most of the studies mentioned above have focused on the *seasonal* response to precessional forcing, while the mechanisms driving precessional changes in *annual mean* precipitation have received less attention. This nonetheless poses an interesting question, given the fact that precession only changes the strength of the seasonal cycle, and not annual mean insolation. Any change in annual mean climate on precessional timescales must therefore come about through nonlinear rectification processes (Huybers and Wunsch 2003; Rial et al. 2004; Laepple and Lohmann 2009; Merlis et al. 2013). Here we illustrate the concept of nonlinear rectification by looking at the role of clouds in rectifying changes in surface shortwave radiation.

Suppose that we have two realizations of the climate system, whose variables  $x_1$  and  $x_2$  differ both in their annual mean (denoted by a bar) and average seasonal cycle (denoted by angle brackets):

$$\begin{aligned} x_1(\tau) &= \bar{x}_1 + \langle x_1 \rangle(\tau) \\ x_2(\tau) &= \bar{x}_2 + \langle x_2 \rangle(\tau), \text{ and} \end{aligned} \quad (1)$$

$$\delta x(\tau) = x_1(\tau) - x_2(\tau), \quad (2)$$

where  $\tau$  captures the seasonal time-evolution. The variable under consideration is shortwave radiation at the surface,  $Q_{SW}$ , which is less than shortwave radiation at the top of the atmosphere (TOA),  $Q_{IN}$ , due to reflection by the surface and cloud albedo,  $\alpha_S$  and  $\alpha_C$ , respectively:

$$Q_{SW,i}(\tau) = (1 - \bar{\alpha}_S)(1 - \alpha_{C,i}(\tau))Q_{IN,i}(\tau), \quad i = 1, 2 \quad (3)$$

where

$$\alpha_{C,i}(\tau) = \bar{\alpha}_{C,i} + \langle \alpha_{C,i} \rangle(\tau), \quad (4)$$

and for simplicity we have assumed that  $\alpha_S$  does not change seasonally and between climate states. Here we ignore absorption of shortwave radiation in the atmosphere. The difference in surface shortwave radiation between the two climate states is given by:

$$\begin{aligned} \delta Q_{SW} &= Q_{SW,1}(\tau) - Q_{SW,2}(\tau) \\ &= (1 - \bar{\alpha}_S)(1 - \alpha_{C,1}(\tau))Q_{IN,1}(\tau) \\ &\quad - (1 - \bar{\alpha}_S)(1 - \alpha_{C,2}(\tau))Q_{IN,2}(\tau). \end{aligned} \quad (5)$$

In this manuscript we will study two realizations of the climate system in the Community Earth System Model (CESM) 1.0.3: a simulation using maximum precession,  $P_{MAX}$ , and a simulation using minimum precession,  $P_{MIN}$ . Details of these experiments are described in Sect. 2. Figure 2a, c—for illustrative purposes—show the zonal mean seasonal cycle and annual mean of  $Q_{IN,P_{MIN}}$  and  $Q_{SW,P_{MIN}}$  respectively. The zonal mean precessionally-induced changes in TOA and surface shortwave radiation,

$[\delta Q_{IN}]$  and  $[\delta Q_{SW}]$ , are shown in Fig. 2b, d. While there is no precessional change in zonal annual mean TOA insolation  $[\delta Q_{IN}]$  (Fig. 2b), there is a substantial non-zero annual mean change in zonal mean surface insolation  $[\delta Q_{SW}]$  of more than 10 W/m<sup>2</sup> (Fig. 2d).

To assess the contributors to the annual mean surface insolation changes  $[\delta Q_{SW}]$  in Fig. 2d, we calculate the annual mean of the individual terms contributing to Eq. (5). Realizing that  $\bar{x}\langle y \rangle = \bar{x}\langle y \rangle = 0$  and that for precession  $\delta \bar{Q}_{IN} = 0$ , only four terms contribute to annual mean surface insolation changes:

$$\begin{aligned} [\delta Q_{SW}] &= - \left[ (1 - \bar{\alpha}_S) \overline{\langle \alpha_C \rangle_{P_{MIN}}} \delta \langle Q_{IN} \rangle \right] \quad (A) \\ &\quad - \left[ (1 - \bar{\alpha}_S) \delta \langle \alpha_C \rangle \langle Q_{IN} \rangle_{P_{MIN}} \right] \quad (B) \\ &\quad - \left[ (1 - \bar{\alpha}_S) \delta \langle \alpha_C \rangle \delta \langle Q_{IN} \rangle \right] \quad (C) \\ &\quad - \left[ (1 - \bar{\alpha}_S) \delta \bar{\alpha}_C \overline{Q_{IN,P_{MIN}}} \right] \quad (D) \end{aligned} \quad (6)$$

These terms are shown for the zonal mean in Fig. 2d. The dominant contributor to  $[\delta Q_{SW}]$  is term D in Eq. (6), the combination of annual mean cloud changes ( $\delta \bar{\alpha}_C$ ) and longterm mean insolation ( $\overline{Q_{IN,P_{MIN}}}$ ). The other terms, rectification of anomalous insolation by mean clouds (A), rectification of mean insolation by anomalous clouds (B), and rectification of anomalous insolation by anomalous clouds (C), all contribute several W/m<sup>2</sup> each, but are of opposite sign and thus largely cancel in the zonal mean.

The aim of this paper is to identify the key mechanisms that rectify the zero-annual mean precessional forcing into an annual mean tropical precipitation response. Merlis et al. (2013) previously studied such nonlinear rectification mechanisms using idealized experiments in an aquaplanet model. They found the main nonlinearity to be a thermodynamic one, relating to the covariance of the climatological seasonal cycle of the meridional circulation with the seasonal changes in specific humidity (see their Fig. 1). This study however did not take into account the role of continents, changes in clouds, or ocean circulation. Here we look for nonlinear mechanisms rectifying the response of annual mean precipitation to seasonal precessional forcing in a more realistic modeling framework. We find that the dynamical (mean circulation) response to precessional insolation changes far outweighs the thermodynamic response, suggesting that the Merlis et al. (2013) idealized modeling setup may not translate to the real world. While in our study the zonal annual mean precipitation change follows the traditional view of the warmer summer hemisphere getting wetter, regional responses diverge widely. The highly regional nature of tropical hydroclimate processes impedes the identification of a universal tropical rectification mechanism. We therefore focus on a specific region, the Atlantic intertropical convergence zone (ITCZ), which has been the subject of various paleoclimate



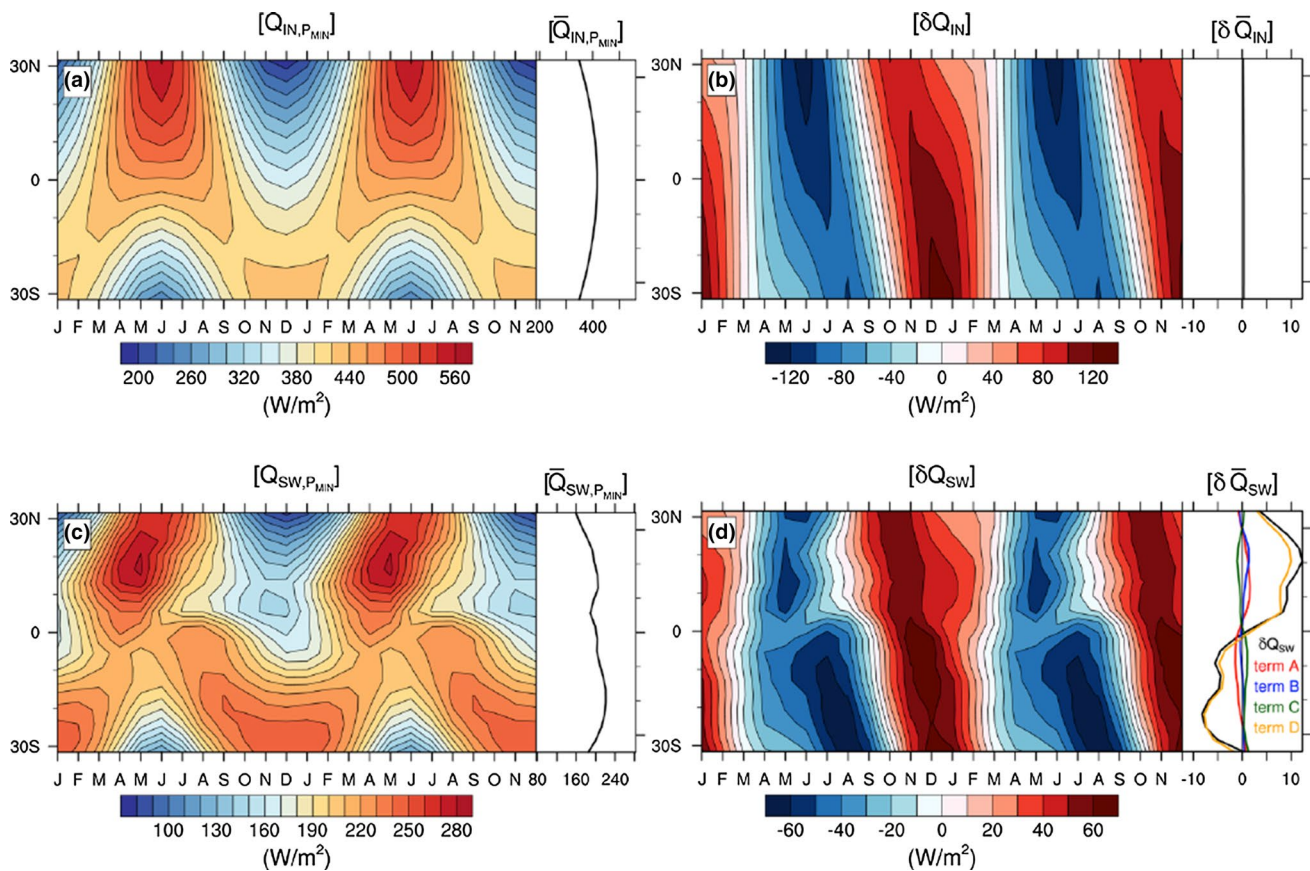


**Fig. 2** Top: Zonal mean shortwave radiation at the top of the atmosphere for (a)  $P_{\text{MIN}}$  ( $[Q_{\text{IN}}]$ ) and (b)  $P_{\text{MAX}} - P_{\text{MIN}}$  ( $[\delta Q_{\text{IN}}]$ ); Bottom: Zonal mean surface shortwave radiation for (c)  $P_{\text{MIN}}$  ( $[Q_{\text{SW}}]$ ) and

(d)  $P_{\text{MAX}} - P_{\text{MIN}}$  ( $[\delta Q_{\text{SW}}]$ ). Insets on the right show the annual mean change. A detailed description of these various terms can be found in Sect. 1

reconstruction efforts (Arbuszewski et al. 2013; Deplazes et al. 2013).

Previous (paleo-)modeling and observational work has found that the Atlantic ITCZ is highly sensitive to changes in the cross-equatorial sea-surface temperature (SST) gradient (Lindzen and Nigam 1987; Chiang et al. 2002), and responds to a variety of local and remote forcings. These include diabatic heating over the African continent (Biasutti et al. 2005), interannual variability in the Pacific and North Atlantic (Marshall et al. 2001; Chiang et al. 2002), high-latitude changes in sea ice and ice sheets (Chiang et al. 2003; Chiang and Bitz 2005; Broccoli et al. 2006; Marzin et al. 2013), and changes in the AMOC (Timmermann et al. 2007; Deplazes et al. 2013). Here we propose that the response of the Atlantic ITCZ to precessional forcing is strongly impacted by changes in temperature and precipitation over the surrounding continents. The African and South American land surface response to precessional forcing as well as the ability of the continents to alter the oceanic ITCZ are both seasonally dependent and thus serve as important annual rectifying processes of precipitation over the tropical Atlantic.

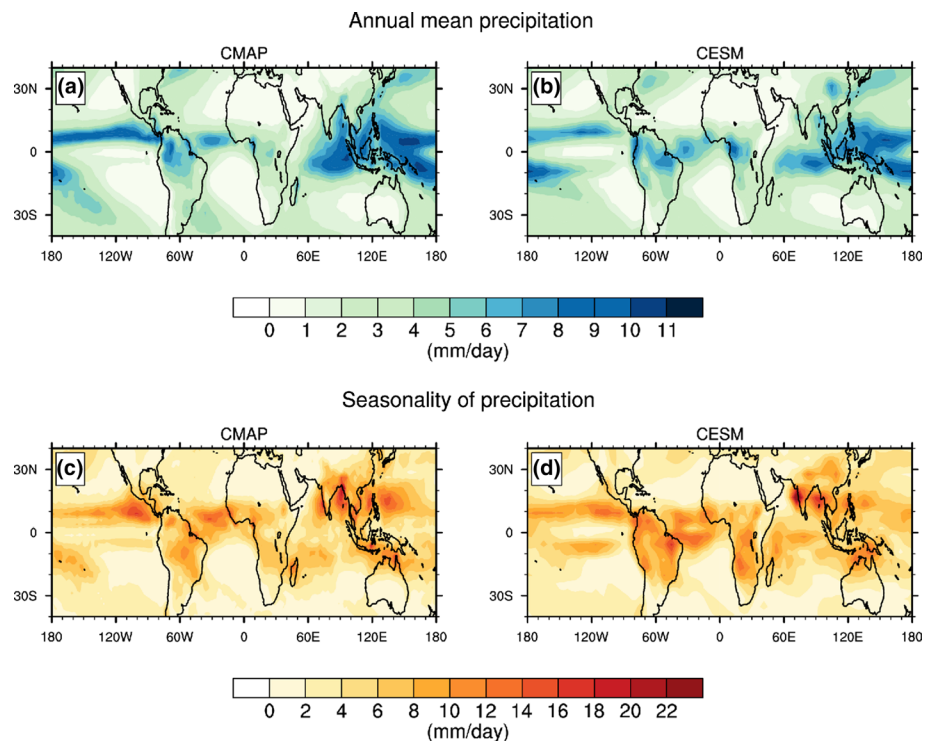
Section 2 gives a detailed description of our modeling setup. In Sect. 3.1 the large-scale patterns of annual mean tropical precipitation change associated with precessional forcing are presented. Section 3.2 focuses on the Atlantic ITCZ and discusses how the continental response to precessional forcing rectifies the response of the Atlantic ITCZ. Our results are compared against paleoclimate reconstructions from Cariaco Basin (Deplazes et al. 2013), Brazil (Wang et al. 2004, 2007; Cruz et al. 2005), and the tropical Atlantic (Tjallingii et al. 2008; Arbuszewski et al. 2013) in Sect. 4, where we will also briefly touch on the role of eccentricity. Section 5 summarizes and concludes this work.

## 2 Methods

To study the response of annual mean tropical climate to precessional forcing, we performed two equilibrium simulations with the Community Earth System Model (CESM) version 1.0.3. This is a fully-coupled, global climate model consisting of interactive atmosphere (CAM4), ocean



**Fig. 3** Annual mean precipitation (*top*) and seasonality of precipitation (maximum minus minimum of monthly climatology; *bottom*) for CMAP monthly climatology (enhanced version, *left*; Xie and Arkin 1997) and CESM1.0.3 pre-industrial control run (*right*; Chikamoto et al. 2015)



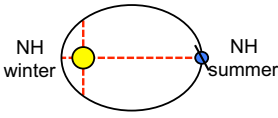
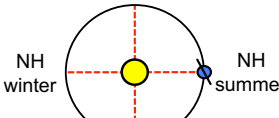
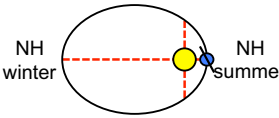
(POP2), sea ice (CICE4) and land (CLM4) components. CESM1 was developed from the Community Climate System Model (CCSM) version 4 (Gent et al. 2011); its enhancements include the incorporation of biogeochemical cycles and atmospheric chemistry (Hurrell et al. 2013; Moore et al. 2013). The atmospheric model was run at T31 resolution, which corresponds to  $3.75^\circ$  by  $3.75^\circ$  horizontal resolution, with 26 vertical levels, while the ocean horizontal resolution is  $3^\circ$  by  $3^\circ$  with 60 vertical levels. This low-resolution version is ideal for performing computationally efficient long equilibrium runs and performs well when compared to higher resolution versions (Shields et al. 2012; Chikamoto et al. 2015; Stevenson et al. 2015). Figure 3 compares tropical annual mean precipitation and seasonality of precipitation of a pre-industrial control run with CESM1.0.3 (Chikamoto et al. 2015) against the CPC Merged Analysis of Precipitation (CMAP) NCEP Reanalysis-enhanced monthly climatology (Xie and Arkin 1997). CESM captures the dominant features of annual mean precipitation and seasonality; its main deficiencies are an underestimation of the tilt of the South Pacific Convergence Zone and annual mean precipitation over the Indian Ocean. The overestimation of Atlantic precipitation seasonality south of the equator is a result of Atlantic mean state biases common amongst CMIP5 GCMs, which simulate a reversal of the annual mean SST gradient and a boreal spring westerly wind bias (e.g. Richter et al. 2014; Siongco et al. 2014). Richter et al. (2012) attribute this wind bias to precipitation deficits over the Amazon basin and excess

precipitation over the Congo basin, also seen for CESM in Fig. 3.

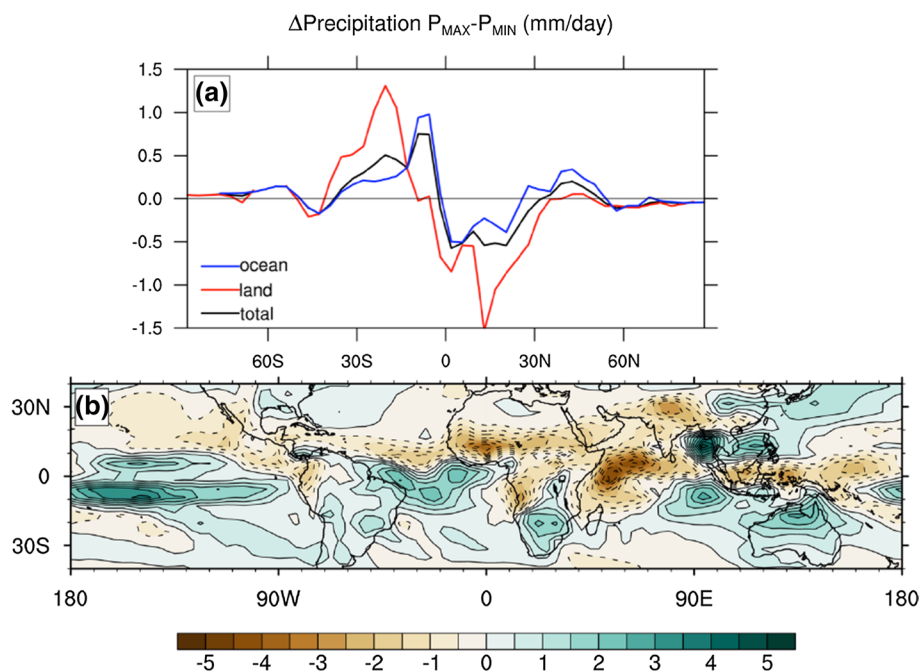
The precessional experiments use two extreme phases of precession: one with perihelion occurring in Northern Hemisphere (NH) winter solstice ('maximum precession',  $P_{\text{MAX}}$ ), and one with perihelion occurring in NH summer solstice ('minimum precession',  $P_{\text{MIN}}$ ). For the precessional parameter we use the definition of precession used by Paillard (2001) and others, where  $\omega = \pi + \tilde{\omega}$ , with  $\tilde{\omega}$  the angle between the vernal equinox and perihelion. As noted before, the strength of the precessional forcing is modulated by eccentricity  $e$ . To maximize the effects of precession on climate we therefore increase the value of eccentricity to  $e = 0.067$ , the maximum value during the past 51 million years (51 Ma) (Laskar et al. 2004). Pre-industrial greenhouse gas concentrations and obliquity were used. The simulations were started from an equilibrated pre-industrial control run (Chikamoto et al. 2015) and run for 500 years. The climatologies used in our analysis are linearly detrended averages over the years 201–500. Results in this paper will generally be presented as maximum minus minimum precession,  $P_{\text{MAX}} - P_{\text{MIN}}$ .

An additional run was performed with eccentricity set to zero ( $E_{\text{ZERO}}$ ). In this run the orbit of the earth around the sun is perfectly circular, and there is thus no hemispheric difference in seasonal cycle strength. The results of this run will be used in Sect. 4 where we discuss rectification due to eccentricity. A summary and illustration of all three runs is given in Table 1.

**Table 1** Overview of the experimental setup for the simulations with CESM1.0.3

$P_{MAX}$ <i>Maximum precession</i>	$E_{ZERO}$ <i>Zero eccentricity</i>	$P_{MIN}$ <i>Minimum precession</i>
		
$\omega = 270^\circ$	Precession does not matter	$\omega = 90^\circ$
$e = 0.067$	$e = 0$	$e = 0.067$
NH summer solstice in aphelion	Aphelion = perihelion	NH summer solstice in perihelion

All experiments use pre-industrial CO<sub>2</sub> (284.7 ppmv), and present-day obliquity 23.4°. Simulations were run for 500 years, and climatologies were calculated over the linearly detrended last 300 years of the run

**Fig. 4** Annual mean  $P_{MAX} - P_{MIN}$  difference in precipitation (mm/day) for **a** zonal mean, separated by ocean (blue), land (red), and total (black); **b** spatial pattern in the tropics

### 3 Results

#### 3.1 The tropical precipitation response to precessional forcing

The general picture that emerges from the, essentially terrestrial, proxy-estimates shown in Fig. 1 is that maximum precipitation in the tropics follows local maximum summer insolation. When considering the annual, zonal mean change in net precipitation in our model simulations (Fig. 4a) a similar view emerges: in the  $P_{MAX}$  run the tropical precipitation maximum shifts towards the Southern Hemisphere, which has a stronger SH seasonal cycle than

the  $P_{MIN}$  run. This is true for precipitation over land as well as over the ocean. While the oceanic precipitation change is mostly confined between 15°S and 15°N, and switches sign roughly at the equator, continental precipitation changes have a larger meridional extent due to the strong contributions of landmasses located away from the equator (e.g. Australia, South Africa, the Himalayas) and (in the zonal mean) switch from positive to negative around 10°S.

A better understanding of regional processes is obtained by studying the spatial distribution of the annual mean precessional precipitation changes (Fig. 4b). The regional hydroclimate responses are clearly much more complex than just the warmer summer hemisphere (SH, for  $P_{MAX}$ )

**Table 2** Seasonally and annually integrated  $P_{MAX}-P_{MIN}$  difference in total precipitation ( $m^3$  and %) over the South American continent ( $80^\circ W-40^\circ W$ ,  $30^\circ S-10^\circ N$ ), Atlantic Ocean ( $60^\circ W-20^\circ E$ ,  $20^\circ S-20^\circ N$ ) and African continent ( $10^\circ W-30^\circ E$ ,  $30^\circ S-30^\circ N$ )

	South America		Atlantic		Africa	
	$m^3$	%	$m^3$	%	$m^3$	%
DJF	$2.29 \times 10^{12}$	36.2	$-1.91 \times 10^{12}$	-32.9	$2.59 \times 10^{12}$	85.9
MAM	$-4.67 \times 10^{11}$	-7.0	$2.38 \times 10^{12}$	47.5	$-1.75 \times 10^{12}$	-35.2
JJA	$-8.46 \times 10^{11}$	-22.2	$3.48 \times 10^{12}$	66.7	$-5.51 \times 10^{12}$	-81.1
SON	$6.81 \times 10^{11}$	10.8	$-1.66 \times 10^{12}$	-24.4	$1.92 \times 10^{11}$	4.1
Annual	$1.66 \times 10^{12}$	7.2	$2.28 \times 10^{12}$	10.0	$-4.38 \times 10^{12}$	-22.4

becoming wetter. We find a small intensification of the SH monsoon systems (South America, Southern Africa and Australia), and a decrease in precipitation over the South and East Asian monsoon regions. The annual mean ITCZ over the Atlantic shifts towards the warmer summer hemisphere as well. But over the Pacific, there is an increase in precipitation over the northern equatorial Pacific (dateline to  $110^\circ W$ ) in addition to a strong intensification south of the equator. The latter appears to be related to a reduction in the tilt of the South Pacific Convergence Zone. The wettening of the central Pacific is contrasted zonally with a drying of the Western Warm Pool region. Over the Indian Ocean there is a dipole pattern with a meridionally slanted zero-line. Finally there is a strong increase in annual mean precipitation over the Andaman and South China Seas. All together, Fig. 4b shows that the simple paradigm of precipitation shifting towards the warmer summer hemisphere (SH in  $P_{MAX}$ )—although valid in a zonal mean sense—does not apply universally throughout the tropics. Zonal mean frameworks of understanding the ITCZ, such as the ones discussed by Schneider (1977), Lindzen and Hou (1988), Kang et al. (2009) and Schneider et al. (2014), will therefore not be able to explain the regional changes in tropical precipitation.

### 3.2 The Atlantic ITCZ

#### 3.2.1 Position versus intensity

The differential response across the tropics of precipitation to precessional forcing suggests that regional dynamics play an important role, and it will not be possible to find a universal mechanism driving this response. In the remainder of this paper we will therefore focus our attention on one specific region, the Atlantic ITCZ. Throughout the literature, different definitions of the ITCZ are used; here we take ITCZ to refer to either the location of maximum precipitation or the location of zero meridional wind (confluence line).

Despite an annual mean insolation profile that is symmetric around the equator, the present-day climatological annual mean ITCZ over the Atlantic Ocean is displaced

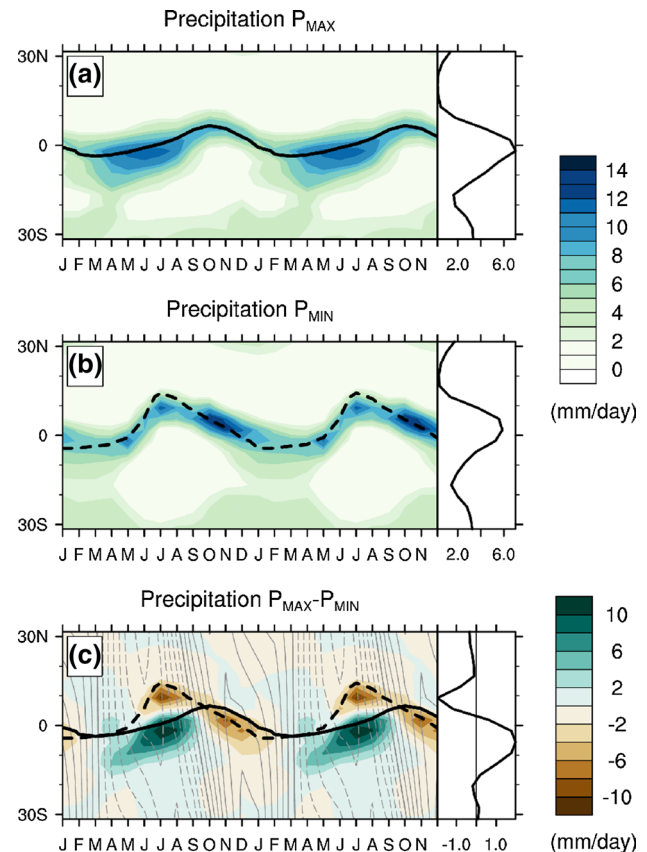


**Fig. 5** Zonal mean precipitation (mm/day) over the Atlantic ( $40^\circ-20^\circ W$ ) for **a**  $P_{MAX}$ ; **b**  $P_{MIN}$ ; **c**  $P_{MAX}-P_{MIN}$ . The black line indicates the position of the ITCZ as measured by the location of zero meridional wind speed for  $P_{MAX}$  (solid) and  $P_{MIN}$  (dashed). Insets on the right show the corresponding annual mean  $P_{MAX}-P_{MIN}$  TOA insolation, as in Fig. 2b

into the Northern Hemisphere (e.g. Mitchell and Wallace 1992). While the question of the hemispheric preference of the ITCZ has not been answered definitively, it has been attributed to the existence of the AMOC (e.g. Krebs and Timmermann 2007; Schneider et al. 2014) as well as the asymmetry of the continents surrounding the Atlantic Ocean and its resulting ocean-atmosphere interactions (Xie 1996, 2005; Xie and Saito 2001). Seasonally the Atlantic ITCZ migrates from a position close to the equator in



boreal spring to a maximum northward position around 10°N in late summer (e.g. Mitchell and Wallace 1992). This seasonal march of the ITCZ has been found to be sensitive to remote climate forcing on various timescales, such as the El Niño–Southern Oscillation (Chiang et al. 2002), the North Atlantic Oscillation (Marshall et al. 2001), Northern Hemisphere ice conditions (Chiang et al. 2003; Chiang and Bitz 2005; Broccoli et al. 2006), the Atlantic meridional mode (Nobre and Shukla 1996; Chiang et al. 2002; Xie and Carton 2004), and meltwater pulses and AMOC (Broccoli et al. 2006; Timmermann et al. 2007; Deplazes et al. 2013; Marzin et al. 2013; Menviel et al. 2014).

As noted in Sect. 3.1, the annual mean Atlantic ITCZ responds to precession by shifting towards the warmer summer hemisphere (Fig. 4b), with more precipitation under  $P_{\text{MAX}}$  forcing occurring in the south, and less in the north. The resulting dipole is not centered on the equator, nor is it symmetric around its axis. Rather, the increase in precipitation on the southern side of the dipole is stronger than the decrease on its northern side. In the  $P_{\text{MAX}}$  run, total annual integrated precipitation over the Atlantic Ocean between 20°S and 20°N increases by  $2.28 \times 10^{12} \text{ m}^3$ , or 10 % (Table 2). For comparison, global annual integrated precipitation increases by  $2.21 \times 10^{12} \text{ m}^3$ , or 0.5 %

In the context of the precessional forcing, which has a strong seasonal component but no annual one (Fig. 2b), the changes in annual mean precipitation could derive from two components: A change in the seasonal march of the ITCZ (amplitude/position change), or a change in when precipitation occurs along this march (phase change). Figure 5 shows monthly mean precipitation and position of the Atlantic ITCZ as measured by the location of zero meridional wind, averaged between 40°W and 20°W (This longitude range was chosen to isolate the oceanic ITCZ response). In boreal spring and summer, when the  $P_{\text{MIN}}$  insolation in both hemispheres exceeds that of  $P_{\text{MAX}}$  (see Fig. 2b), the ITCZ travels further north, and at an earlier time of year, in the  $P_{\text{MIN}}$  simulation (Fig. 5b) than in the  $P_{\text{MAX}}$  simulation (Fig. 5a). In boreal fall and winter, when the  $P_{\text{MAX}}$  insolation exceeds that of  $P_{\text{MIN}}$ , the reverse does not happen however: The  $P_{\text{MAX}}$  and  $P_{\text{MIN}}$  ITCZs reach approximately the same southward extent. This change in seasonal march of the confluence line—even without a change in seasonality—implies a northward shift of the annual mean Atlantic ITCZ in  $P_{\text{MIN}}$  compared to  $P_{\text{MAX}}$ .

In addition to a change in meridional position, there is a change in phase of the precipitation: Under maximum precession (Fig. 5a), most of the precipitation over the tropical Atlantic falls between April and July, while under minimum precession (Fig. 5b) there are two precipitation maxima—a brief one in July and a more extended one between September and December. The oceanic precipitation maxima

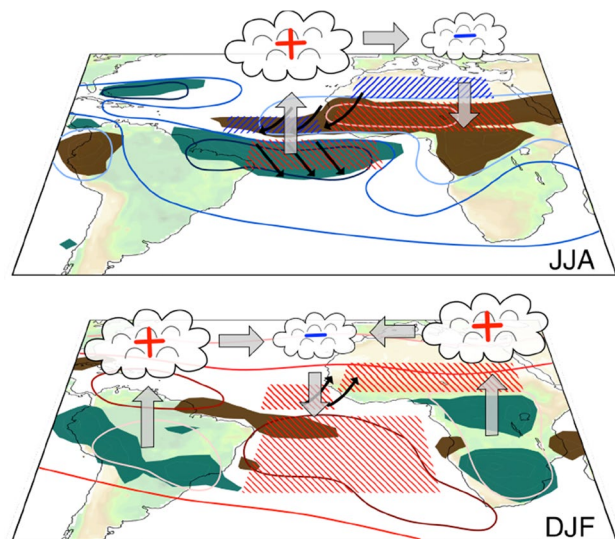


**Fig. 6** Schematic illustrating the main processes affecting the position and intensity of the Atlantic ITCZ for JJA (*top*) and DJF (*bottom*),  $P_{\text{MAX}} - P_{\text{MIN}}$ . Changes in precipitation are indicated by green (*wetter*) and brown (*drier*) shading; contours indicate changes in surface shortwave radiation, with darker colors representing larger changes; red (*left-slanted*) and blue (*right-slanted*) hatching show surface warming and cooling respectively; black arrows indicate changes in surface winds, while grey arrows show changes in vertical circulation

(Fig. 5a, b) thus occur several months after maximum TOA insolation (Fig. 2a).

Different mechanisms are thought to be responsible for driving changes in position and intensity of oceanic moisture convergence in the tropics. Changes in *meridional position* are caused by a mechanism originally proposed by Lindzen and Nigam (1987), relating convergence in the boundary layer to surface pressure gradients caused by meridional (cross-equatorial) SST gradients (see also Tomas et al. 1999). We will refer to this process as the ‘boundary layer mechanism’. An initial meridional displacement can be further amplified by a process known as the Wind-Evaporation-SST (WES) feedback (Xie and Philander 1994): changes in low-level convergence will affect latent heat fluxes and can feed back positively onto the anomalous SST gradient. Numerous studies have shown that the WES feedback is an important amplifier of meridional ITCZ shifts over the Atlantic Ocean (e.g. Braconnot et al. 2000; Biasutti et al. 2005; Zhao et al. 2005; Bosmans et al. 2012).

On the other hand, Gill (1980) and subsequent studies (e.g. Chiang et al. 2001; Biasutti et al. 2004) looked at the entire troposphere, and found that local diabatic forcing can change the stability profile of surrounding areas and drive anomalous adiabatic vertical motion elsewhere, resulting in divergence changes. We will refer to these processes as the

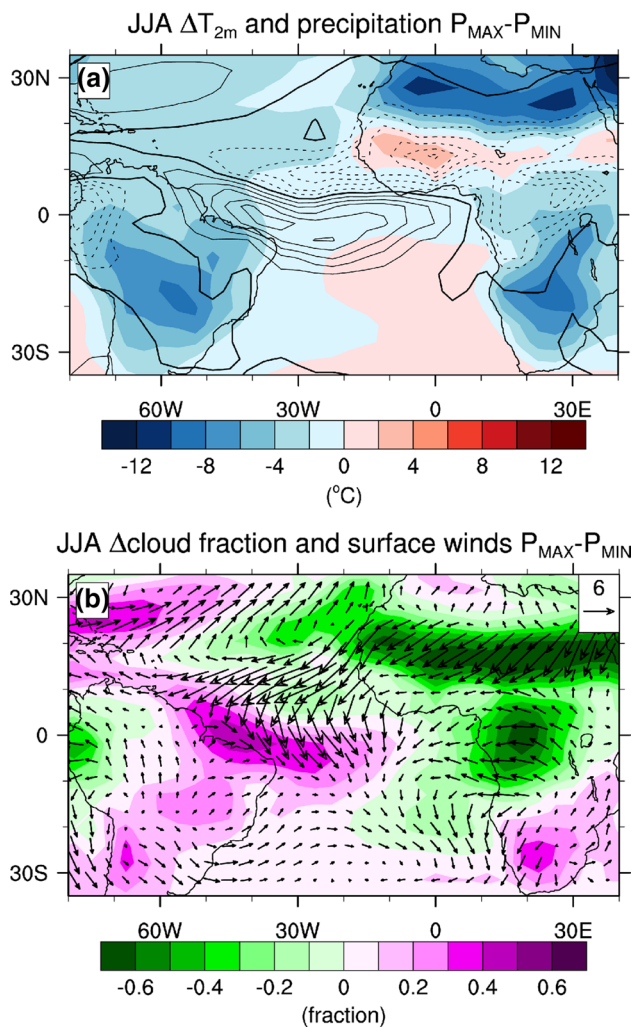


**Fig. 7** JJA  $P_{MAX}-P_{MIN}$  change in **a** 2m temperature (°C; colors) and precipitation (contour levels 2 mm/day); and **b** cloud fraction (colors) and surface winds (m/s; vectors)

‘full troposphere mechanism’. Biasutti et al. (2004, 2005) showed that the precipitation response to remote diabatic forcing depends heavily on the background stability of the troposphere. Changes in diabatic heating are most likely to induce remote changes in regions where there is already precipitation occurring. The full troposphere mechanism therefore mostly impacts the *intensity* of precipitation.

In the following sections we more closely evaluate the precipitation response in individual seasons to see what drives precessional changes in the intensity and meridional position of the ITCZ. The main results are summarized schematically in Fig. 6. We argue that the precessional precipitation response over the Atlantic Ocean is a direct result of continental forcing. The continental response to precessional forcing, and the oceanic response to these continental changes, vary in time and space and thus rectify the annual mean change of the Atlantic ITCZ.

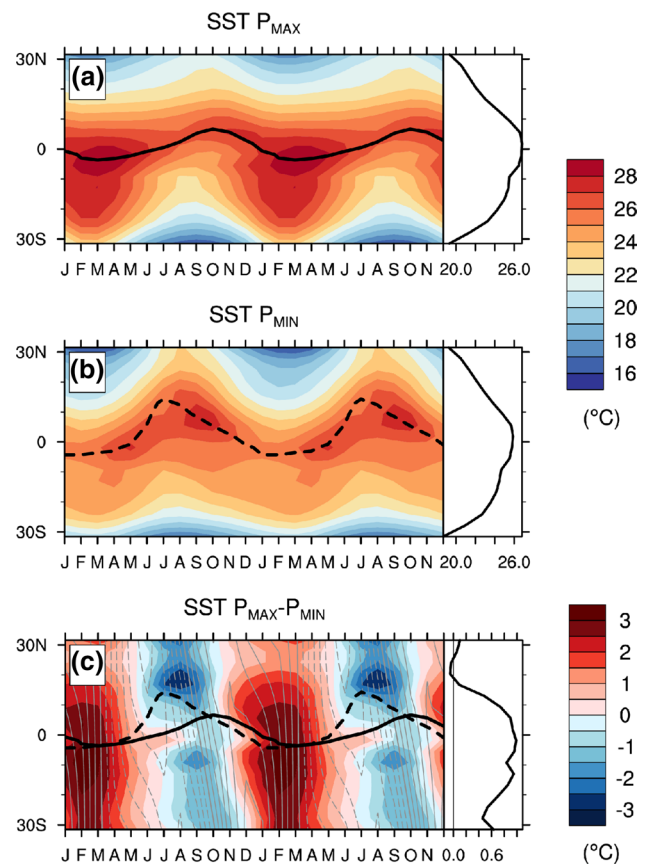
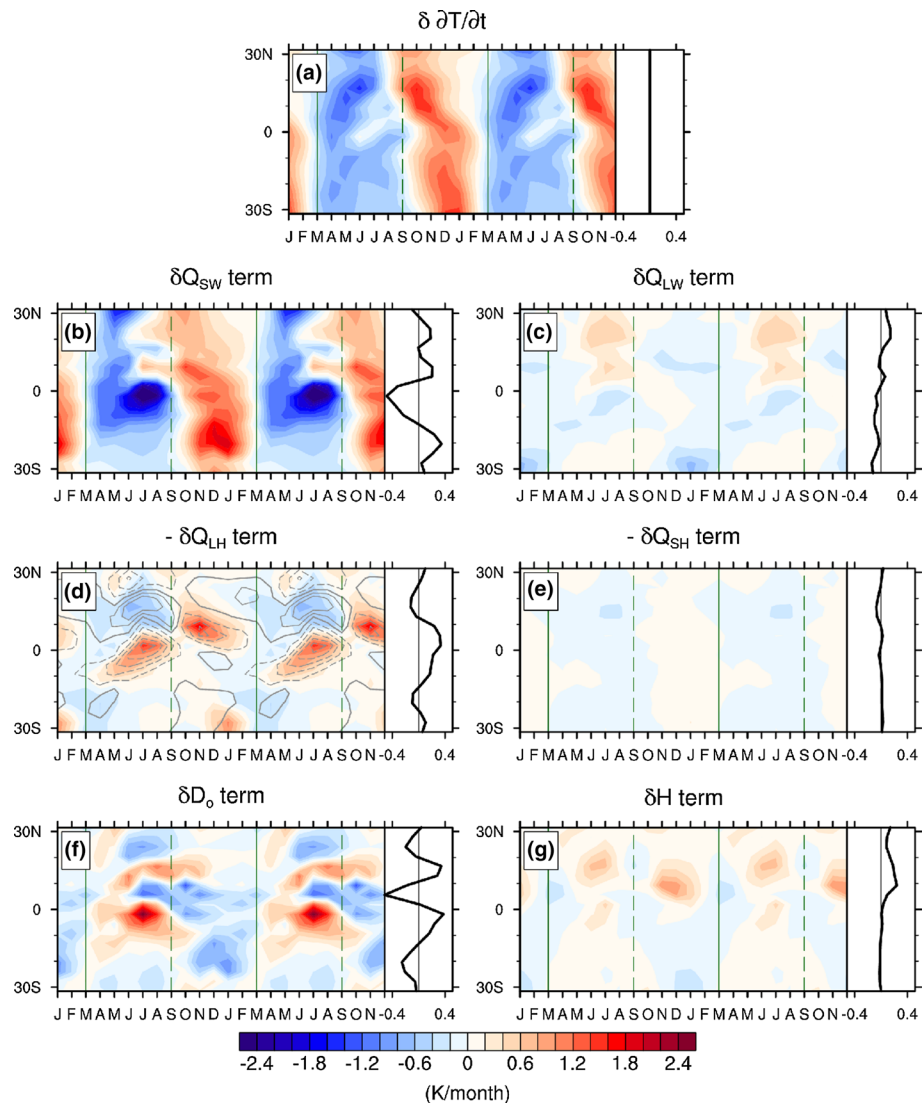


**Fig. 8** Zonal mean SST (°C) over the Atlantic (40°–20°W) for **a**  $P_{MAX}$ ; **b**  $P_{MIN}$ ; **c**  $P_{MAX}-P_{MIN}$ . The black line indicates the position of the ITCZ as measured by the location of zero meridional wind speed for  $P_{MAX}$  (solid) and  $P_{MIN}$  (dashed). Insets on the right show the corresponding annual mean. Contours in (c) show  $P_{MAX}-P_{MIN}$  TOA insolation, as in Fig. 2b

### 3.2.2 The JJA ITCZ

In JJA, precipitation over the Atlantic Ocean in  $P_{MAX}$  increases between 5°S–5°N, while it decreases between 5°N and 10°N (Fig. 7a, contours). These simulated changes in precipitation could be driven by temperature-induced changes in specific humidity (‘thermodynamics’), by changes in the mean circulation (‘dynamics’), by changes in transient eddy moisture convergence or by changes in evaporation. While Merlis et al. (2013) in an aquaplanet simulation attributed precessionally induced changes in the ITCZ mostly to thermodynamic processes, a decomposition of the moisture budget in our simulations (along the lines of e.g. Trenberth and Guillemot 1995; Clement et al. 2004; Held and Soden 2006; Seager et al. 2010) indicates that the dominant contribution to JJA precipitation changes over the Atlantic are changes in the mean circulation, in particular its convergence (see “Appendix”). We suggest that in this season, the meridional

**Fig. 9** Zonal mean contributions to the  $P_{MAX}-P_{MIN}$  change in heating rate (K/month) of the Atlantic Ocean (40°–20°W) mixed layer (a), from (b) a change in shortwave radiation; c a change in longwave radiation; d a change in latent heat flux (negative plotted); e a change in sensible heat flux (negative plotted); f changes in advection and mixing; g changes in mixed layer depth; see Eq. (9). *Insets* on the *right* show the corresponding annual mean; *green lines* indicate the March (*solid*) and September (*dashed*) months for reference. *Contours* in (d) show  $P_{MAX}-P_{MIN}$  wind speed



position of the Atlantic ITCZ is impacted by surface temperature changes over Africa, while its intensity is affected by changes in the African summer monsoon.

Between March and August there is a  $P_{MAX}$ -induced anomalous reduction in TOA shortwave radiation throughout the entire tropics (Fig. 2b). Figure 7a shows the resulting changes in JJA 2m temperature and precipitation. Over northern Africa (20°N), where climatological soil moisture is low, the reduction in insolation leads to strong continental cooling. South of 20°N, it causes a weakening of the climatological African summer monsoon and equatorial precipitation: total precipitation over the African continent in  $P_{MAX}$  is reduced by 35 % in MAM and 81 % in JJA (see Table 2; Fig. 7a). This weakening is accompanied by a reduction in cloudiness (Fig. 7b) and evaporative cooling that creates a net surface forcing opposite in sign to the original TOA forcing. This results in a reduction of the  $P_{MAX}$  cooling between 10°S–10°N, and even a slight warming between 10°N–20°N (Fig. 7a).

As shown by Chiang et al. (2001), the North Atlantic trade winds strongly respond to remote influences such as ENSO and continental forcing (unlike the Atlantic cross-equatorial winds, which are very sensitive to changes in the cross-equatorial SST gradient). The reduction of continental temperatures over northern Africa drives wind changes that advect dry air southward, and strengthen the North Atlantic trades in  $P_{MAX}$  (Fig. 7b). This intensification of the trade winds sets up an anomalous meridional SST gradient that alters the meridional position of the Atlantic ITCZ through the boundary layer mechanism.

Figure 8 shows the  $P_{MAX}$  and  $P_{MIN}$  zonal mean Atlantic SSTs and their difference, averaged between 40°W and 20°W. Generally the maximum precipitation, maximum SST and the confluence line are closely co-located, with the notable exception of  $P_{MIN}$  JJA, when the precipitation maximum is located in between the confluence line and SST maximum (Figs. 5, 8). Previous work has indicated



that SST and precipitation maxima do not co-locate when meridional pressure gradients play an important role in driving moisture convergence (e.g. Tomas and Webster 1997). Indeed, Fig. 8c indicates that the anomalous northward ITCZ shift in  $P_{\text{MIN}}$  JJA coincides with the onset of an anomalous meridional SST gradient.

The role of the strengthening trade winds in driving the onset of this anomalous meridional SST gradient can be illustrated through a calculation of the mixed layer heat budget. The time evolution of the vertically integrated mixed layer temperature is given by the SST equation:

$$c_p \rho_0 H \frac{\partial T}{\partial t} = D_o + Q_{\text{net}} \quad (7)$$

$$= D_o + Q_{\text{SW}} + Q_{\text{LW}} + Q_{\text{LH}} + Q_{\text{SH}}.$$

Here  $T$  is SST,  $c_p$  is the specific heat capacity at constant pressure,  $\rho_0$  the density of seawater, and  $H$  the seasonally and spatially varying mixed layer depth.  $Q_{\text{SW}}$ ,  $Q_{\text{LW}}$ ,  $Q_{\text{LH}}$ , and  $Q_{\text{SH}}$  are the surface heat fluxes from shortwave and longwave radiation, latent heat and sensible heat respectively.  $D_o$  represents the changes in mixed layer temperature due to ocean heat transport (three-dimensional advection and mixing). We can calculate the change in mixed layer heating rate from

$$\delta \left( c_p \rho_0 H \frac{\partial T}{\partial t} \right) = \delta Q_{\text{SW}} + \delta Q_{\text{LW}} + \delta Q_{\text{LH}} + \delta Q_{\text{SH}} + \delta D_o, \quad (8)$$

which after some manipulation becomes

$$\delta \frac{\partial T}{\partial t} = \frac{1}{c_p \rho_0 H_{P_{\text{MAX}}}} \{ \delta Q_{\text{SW}} + \delta Q_{\text{LW}} + \delta Q_{\text{LH}} + \delta Q_{\text{SH}} + \delta D_o \} - \frac{\delta H}{H_{P_{\text{MAX}}}} \left( \frac{\partial T}{\partial t} \right)_{P_{\text{MIN}}}, \quad (9)$$

where  $\delta$  is the difference operator  $P_{\text{MAX}} - P_{\text{MIN}}$ .

Figure 9 shows these various contributions to the change in heating rate. Note that the negative latent heat and sensible heat flux changes are plotted so that blue and red correspond to cooling and heating respectively. The ocean heat transport term in Fig. 9f was calculated as the residual from the surface heat fluxes and the  $c_p \rho_0 H \frac{\partial T}{\partial t}$  term. Over the ocean, there is generally a 1–2 month lag between insolation forcing and surface temperature changes. In order to understand the onset of the anomalous SST gradient in May, as seen in Fig. 8c, we therefore need to understand the contributions to  $\delta \frac{\partial T}{\partial t}$  in March (referenced by the solid green line in Fig. 9).

The TOA insolation forcing shown in Fig. 2b shows little meridional gradient in boreal spring. At the surface, net shortwave radiation  $\delta Q_{\text{SW}}$  (Fig. 9b) shows a strong cooling between 20°S and 10°N which is due to a  $P_{\text{MAX}}$  increase in

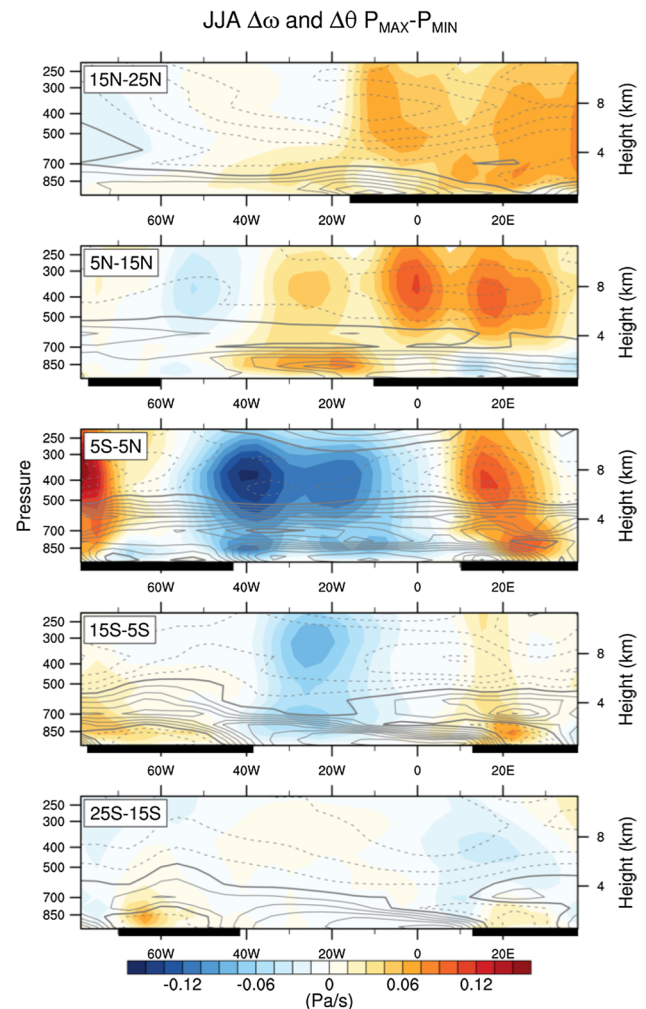


**Fig. 10** JJA  $P_{\text{MAX}} - P_{\text{MIN}}$  change in vertical velocity (Pa/s; colors) and potential temperature anomalies with respect to the vertical average (contour levels 0.5 °C) for various latitude bands across the tropical Atlantic: **a** 15°N–25°N; **b** 5°N–15°N; **c** 5°S–5°N; **d** 15°S–5°S; **e** 25°S–15°S. Black bars indicate land

cloudiness over these latitudes (Fig. 7b) following the precipitation changes of Fig. 5c. By contrast, the total anomalous heating rate plotted in Fig. 9a shows strongest cooling in boreal spring over the North Atlantic. This cooling is the result of an anomalous  $P_{\text{MAX}}$  increase in the surface latent heat flux (Fig. 9d) which cools the North Atlantic starting in March, while a decrease in latent heat flux warms the Atlantic just south of the equator. Throughout boreal spring and summer, the changes in latent heat flux continue to warm the Atlantic south of 5°N and cool it north of that in  $P_{\text{MAX}}$ . The dipole in latent heat flux changes is formed by the  $P_{\text{MAX}}$  strengthening of the trade winds over the North Atlantic, and a weakening of the cross-equatorial winds in boreal spring and summer (Fig. 7b and contours in Fig. 9d). It is a clear indication that the WES feedback is at work: The  $P_{\text{MAX}}$  cooling of the North Atlantic caused by the

boreal spring strengthening of the trades reduces the meridional SST gradient, which keeps the region of convergence close to the equator, weakening the cross-equatorial winds, and warming the equatorial region (Fig. 9d). This warming further reduces the meridional SST gradient (Fig. 8c) and keeps the ITCZ south. The opposite is the case in the  $P_{\text{MIN}}$  simulation, where an increased meridional SST gradient pushes the Atlantic ITCZ north (Fig. 5c).

Coincident with the latent heat flux anomalies, changes in ocean heat transport warm the Atlantic south of  $5^{\circ}\text{N}$  in  $P_{\text{MAX}}$  (Fig. 9f). They further contribute to the  $P_{\text{MAX}}$  weakening of the meridional SST gradient in boreal spring and summer. The longwave, sensible heat, and mixed layer terms of Eq. (9), shown in Fig. 9c, e, and g respectively, contribute little to these heating rate changes. These results thus indicate that through the boundary layer mechanism and amplified by the WES feedback, precessional changes in African temperature and resulting surface wind changes alter the meridional position of the Atlantic ITCZ. While the entire South American continent cools in response to the  $P_{\text{MAX}}$  forcing (Fig. 7a), this cooling does not induce surface wind changes that can impact the ITCZ position (Fig. 7b).

Figure 10 shows JJA cross-sections of vertical velocity changes averaged over various latitude bands. Between  $15^{\circ}\text{S}$  and  $5^{\circ}\text{N}$ , vertical velocity changes over the ocean are opposite in sign to those over the continents (esp. Africa), showing that convection over the ocean decreases when it increases over land. The vertical profile of change in this area is very different from that north of  $5^{\circ}\text{N}$ , where over the Atlantic Ocean ( $50^{\circ}\text{W}$ – $20^{\circ}\text{W}$ ) the response is mostly limited to the boundary layer. Contours in Fig. 10 show potential temperature anomalies with respect to vertical mean changes. Throughout the tropics, the upper troposphere cools compared to the lower troposphere, indicating reduced stability. Together, the vertical velocity and potential temperature changes suggest that the mechanisms described by Biasutti et al. (2004) are at work: the decrease in continental precipitation cools the upper troposphere due to a reduction in diabatic heating, which then reduces the large-scale stability profile and increases convection in areas where the background stability is weak. Between  $5^{\circ}\text{S}$  and  $5^{\circ}\text{N}$ , the diabatic heating (not shown) resulting from the continentally-driven increase in oceanic precipitation partially offsets the large-scale cooling in the upper troposphere. Because climatological precipitation over South America is low in this season, and precessional changes in precipitation are small (Fig. 7a, Table 2), continental changes on the western side of the Atlantic hardly impact the Atlantic ITCZ.

The mechanisms described above are illustrated in the top panel of Fig. 6. The position of the Atlantic ITCZ is affected by  $P_{\text{MAX}}$  continental cooling over northern Africa,

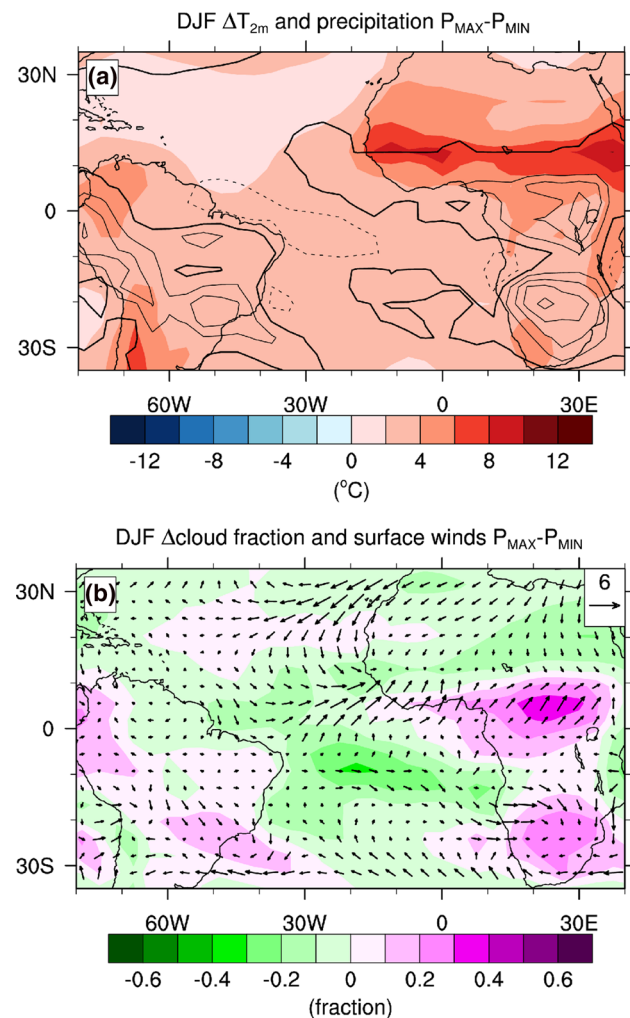


**Fig. 11** DJF  $P_{\text{MAX}}-P_{\text{MIN}}$  change in **a** 2m temperature ( $^{\circ}\text{C}$ ; colors) and precipitation (contour levels 2 mm/day); and **b** cloud fraction (colors) and surface winds (m/s; vectors)

which increases the North Atlantic trades, and through the WES-feedback and wind-induced changes in ocean heat transport reduces the cross-equatorial SST gradient, keeping the  $P_{\text{MAX}}$  ITCZ south. A  $P_{\text{MAX}}$  weakening of the African summer monsoon affects the large-scale stratification profile by cooling the upper troposphere, increasing precipitation in areas that are already unstable, thus changing the intensity of the Atlantic ITCZ. As we shall see in the next section, the magnitude of the processes described above is not seasonally symmetric, thus rectifying the precipitation response in the annual mean.

### 3.2.3 The DJF ITCZ

The response of the Atlantic ITCZ to DJF forcing is markedly different from the JJA changes described above. As seen in Fig. 5, the  $P_{\text{MAX}}$  rainfall maximum attains the

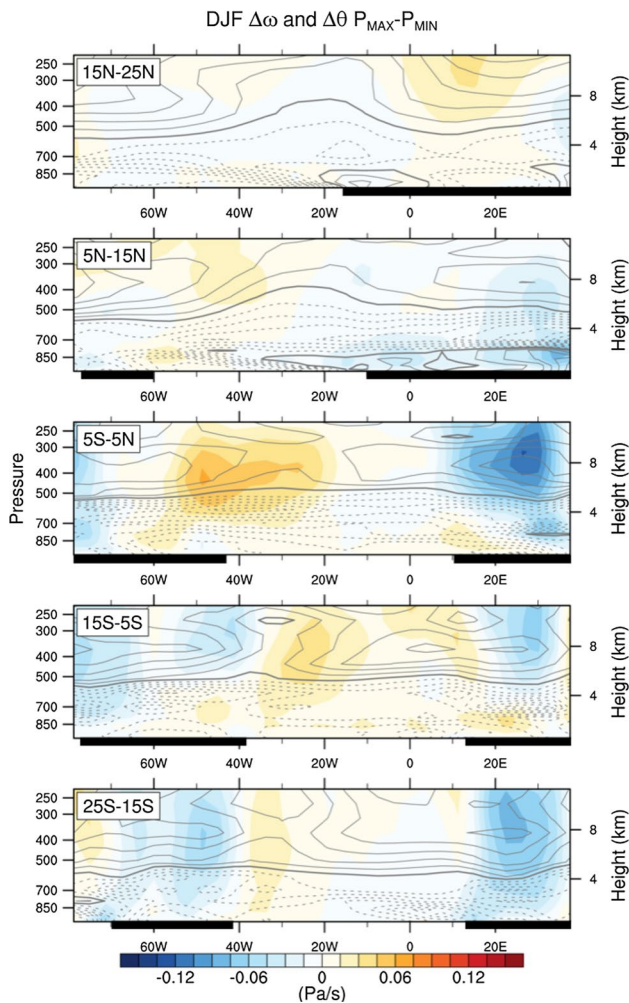


**Fig. 12** DJF  $P_{MAX}-P_{MIN}$  change in vertical velocity (Pa/s; colors) and potential temperature anomalies with respect to the vertical average (contour levels 0.5 °C) for various latitude bands across the tropical Atlantic: **a** 15°N–25°N; **b** 5°N–15°N; **c** 5°S–5°N; **d** 15°S–5°S; **e** 25°S–15°S. Black bars indicate land

same southernmost position as that of  $P_{MIN}$ . Figure 11a shows that in DJF  $P_{MAX}$  precipitation decreases over much of the Atlantic, except close to the African continent. The magnitude of the DJF precipitation response is smaller than that in JJA. An analysis of the DJF moisture budget components indicates that again, the precipitation changes over the ocean are dominated by changes in wind convergence rather than specific humidity (“Appendix”, Fig. 15). Our coupled model simulations suggest that in this season, changes in continental temperature fail to alter trade winds significantly (Fig. 11) and initiate the WES feedback. Changes in precipitation over both Africa and South America affect the intensity of precipitation over the Atlantic but not its location.

The TOA  $P_{MAX}-P_{MIN}$  shortwave forcing in boreal winter (Fig. 2b) is almost the exact mirror image of the

boreal summer forcing. From approximately October to March, incoming shortwave radiation in  $P_{MAX}$  exceeds that in  $P_{MIN}$  throughout the entire tropics, with the strongest forcing over the Southern Hemisphere. In response to this anomalous  $P_{MAX}$  increase in insolation in boreal fall and winter (Fig. 2b), the entire African continent warms up, as shown in Fig. 11a for DJF. Between 10°N–20°N the increase in insolation is amplified by an increase in downward longwave radiation (not shown). South of 10°N, the increase in shortwave radiation leads to an increase in precipitation over the African continent (by as much as 86 % in DJF (Table 2)). As for JJA, precipitation changes over continental Africa in DJF mostly derive from changes in tropospheric convergence, with smaller contributions from evaporation changes and, over southern Africa, a nonlinear and surface term (Fig. 15; see explanation in “Appendix”). The resulting increase in cloudiness (Fig. 11b) and evaporative cooling partially (but not entirely) offset the expected warming (compare Figs. 7a, 11a).

The positive  $P_{MAX}$  shortwave forcing enhances the austral summer monsoon over South America. Total precipitation over the South American continent increases by 36 % in DJF (Table 2). The increase in precipitation largely derives from an increase in wind convergence, but is partially offset by a decrease in moisture advection as increased evaporation over the continent decreases the land-ocean humidity gradient (see “Appendix”, Fig. 15). The entire South American continent warms in response to the positive shortwave forcing (Fig. 11a), although here as well, continental warming is limited by increased cloudiness (Fig. 11b) and latent heat flux.

Even though the  $P_{MAX}$  increase in TOA insolation is strongest over the Southern Hemisphere (Fig. 2b), continental warming is most pronounced over northern Africa (Fig. 11a). This warming causes a thermal low that slightly weakens the  $P_{MAX}$  North Atlantic trades (Fig. 11b). As evidenced by the heat flux analysis in Fig. 9, this weakening leads to a reduction in oceanic latent heat flux (Fig. 9d) and shallowing of the mixed layer (Fig. 9f) that warm the North Atlantic. This keeps the  $P_{MAX}$  ITCZ north (Fig. 5) at a time when the climatological ITCZ is moving south. At the same time, the southern tropical Atlantic is warming (Fig. 9a) due to the  $P_{MAX}$  increase in shortwave radiation (Fig. 9b). As a result, no meridional heating gradient develops, and the WES-feedback cannot enhance the meridional shift; between December and May the entire tropical Atlantic warms up (Fig. 8c). The overall warming is opposed by ocean heat transport changes (Fig. 9e) that cool the equatorial and South Atlantic. Changes in longwave radiation and sensible heat flux (Fig. 9c, e respectively) again play a negligible role. The boundary layer mechanism that was shown to be essential for the JJA meridional ITCZ shift is thus of minor importance in DJF. This is also shown in



Fig. 12 which shows that there is very little boundary layer response in this season, indicating that a full troposphere response to diabatic heating dominates over the boundary layer mechanism.

Figure 12 shows DJF cross-sections of vertical velocity changes in various latitude bands over the tropical Atlantic. Much like in JJA, vertical velocity changes between 15°S and 5°N over the Atlantic ocean are opposite in sign to those over the continents. The strengthening of the austral summer (DJF) South American and African monsoon systems under maximum precession is associated with increased upward motion over land, in particular over Africa between 5°S and 5°N (Fig. 12). The associated convective heating (not shown) warms the upper troposphere (contours in Fig. 12), making it more stable and reducing convection over the ocean in  $P_{\text{MAX}}$  (Figs. 5, 11a). Biasutti et al. (2004) showed that convection changes over South America and southern Africa play comparable roles in driving precipitation anomalies in the Atlantic ITCZ. The precipitation changes over the South American and African continents in DJF are smaller than those in JJA (Table 2; Figs. 7a, 11a) so the full troposphere response in this season is weaker as well (compare Figs. 10, 12).

Even though the DJF  $P_{\text{MAX}}-P_{\text{MIN}}$  change in TOA shortwave forcing is almost the exact mirror image of the JJA forcing (Fig. 2b), the ITCZ response to this forcing is markedly different. The mechanisms described in this section are summarized in the bottom panel of Fig. 6. Despite stronger shortwave forcing in the Southern Hemisphere, the strongest continental heating is found over Northern Africa, leading to a slight weakening of the North Atlantic trades and warming of the North Atlantic. Because the South Atlantic is warming at the same time, meridional SST gradients are muted and the WES feedback does not operate. The net effect is that the *position* of the ITCZ does not change. Atlantic precipitation is mostly impacted by an increase in continental precipitation, which through diabatic heating and resulting changes in large-scale stratification decreases the *intensity* of oceanic precipitation.

## 4 Discussion

### 4.1 Nonlinear rectification of the annual mean response

In this study we analyze the response of annual mean precipitation over the Atlantic Ocean to precessional forcing. In an annual mean sense, the precipitation change over the tropical Atlantic (Fig. 4b) seems to be in accordance with the paradigm of the warmer summer hemisphere getting wetter. However, looking at the seasonal response in Fig. 5c, we see that Atlantic precipitation actually *decreases* in the warmer season. Section 3.2 showed that

the response of the Atlantic ITCZ to seasonally symmetric precessional forcing is strongly seasonally asymmetric. We propose that the continents bordering the Atlantic Ocean play a key role in creating this asymmetry (see Fig. 6). The following processes are identified as being responsible for rectifying the annual mean response of the Atlantic ITCZ to precessional forcing:

- The differential continental response to seasonal TOA insolation forcing:
  - The response of the continental monsoon to seasonal insolation changes is much larger in JJA than in DJF (see Table 2; compare Fig. 7a to Fig. 11a and Fig. 10 to Fig. 12). As a result, the continental diabatic forcing affecting the *intensity* of oceanic precipitation will be stronger in JJA as well, skewing the annual mean response. Biasutti et al. (2004) showed that an increase in insolation affects precipitation over different parts of the African continent in different ways: Over southern Africa, it lowers atmospheric stability by causing low-level warming; over North Africa the atmosphere becomes more unstable because increased monsoon flow brings more low-level moisture. Hence, a strengthening of the seasonal cycle in the Northern Hemisphere affects precipitation over Africa differently than a strengthening of the seasonal cycle in the Southern Hemisphere.
  - Figs. 7a and 11a show that the strongest continental temperature response is always found somewhere over northern Africa, even though in DJF the strongest shortwave forcing is over southern Africa. This differential response relates to climatological differences in soil moisture, ground evaporation, and monsoon location.
- The boundary layer mechanism and WES feedback:
  - Chiang et al. (2001) and Xie and Saito (2001) argued that surface winds over the northern tropical Atlantic are more sensitive to continental forcing than winds over the equatorial and southern tropical Atlantic. Under precessional forcing the boundary layer response and resulting WES feedback (Fig. 9d) are therefore stronger in JJA, when the largest shortwave forcing is located in the Northern Hemisphere (Fig. 2b). The right-hand panel of Fig. 9d shows that the latent heat flux contribution to SST changes is strongly rectified in the annual mean, in particular over the North Atlantic.
  - The boundary layer mechanism, shifting the position of the oceanic ITCZ in response to a *seasonally rec-*

tified SST gradient, will also lead to a rectification of the annual mean ITCZ position.

In recent years a framework has emerged in which changes in zonal mean ITCZ position can be diagnosed by looking at inter-hemispheric energy changes and cross-equatorial energy transport. Extratropical heating anomalies in particular, even when zonally bound (Kang et al. 2014), are found to be able to impact the ITCZ position globally, with the ITCZ shifting away from the cooling hemisphere (Broccoli et al. 2006; Kang et al. 2008, 2009; Chiang and Friedman 2012; Donohoe et al. 2013; Schneider et al. 2014). Evidence for a high-latitude forcing of tropical climate comes from numerous modeling and observational studies which suggest that changes in land and sea ice cover, AMOC strength and meltwater pulses all can impact the meridional position of the ITCZ (Chiang et al. 2003; Chiang and Bitz 2005; Timmermann et al. 2007; Deplazes et al. 2013; Fučkar et al. 2013; Marzin et al. 2013; Marshall et al. 2014; Menviel et al. 2014; Deser et al. 2015). Especially sea ice cover is known to be strongly rectified by precessional forcing (Tuentner et al. 2005). In our model simulations we find a strong increase in Northern Hemisphere annual mean sea ice extent under maximum precession, which in this framework would imply a southward shift of the ITCZ.

Kang et al. (2014) recently argued that while regional extratropical cooling can shift the entire ITCZ south, regional heating anomalies in the tropics cause a much more localized ITCZ response. The zonal asymmetry of the tropical precipitation changes shown in Fig. 4b therefore suggests that in response to precession, regional tropical dynamics have a stronger impact on annual mean precipitation than extratropical processes (Clement et al. 2004). Without additional sensitivity experiments however it is not possible to conclusively quantify the relative importance of tropical and extratropical forcings, which in the real climate might well be time-evolving (see discussion below).

In our modeling experiments, vegetation was allowed to respond to the precessionally induced changes in climate. Previous studies have suggested that dynamical vegetation changes can amplify the (continental) precipitation response to precession by altering surface albedo and soil moisture (Tuentner 2004; Clausen et al. 2006; Timm et al. 2010; Koenig et al. 2011). We do indeed find that surface albedo changes in JJA amplify the TOA insolation forcing. However, these changes are small compared to cloud changes (Fig. 7b), so vegetation feedbacks play only a secondary role in our experiments.

## 4.2 Comparison with proxy records

A comparison of our modeling results against reconstructions of past precipitation on precessional time scales is hampered by a number of caveats:

- Precession is not the sole driver of climate variability on long time scales. In addition to the other orbital forcings (eccentricity, obliquity), the glacial cycles of the Pleistocene also saw substantial variations in high latitude (sea) ice volume and extent and atmospheric greenhouse gas concentrations.
- The strength of the precessional forcing is modulated by eccentricity. Over the last glacial cycle, precessional forcing was strongest during MIS5, while it was weakest during MIS2 and 3, at the same time when global ice volume was nearing its peak. The relative importance of precessional forcing will thus vary over the course of the last glacial cycle, while the amplitude of the forcing is always smaller than the idealized forcing applied in this study.
- Reconstructions of past precipitation are not straightforward and all indirect. It is therefore not guaranteed that the proxy records of Fig. 1a all represent *annual mean* precipitation, and not a seasonally weighted signal (e.g. Huybers and Wunsch 2003; Laepple and Lohmann 2009; Timmermann et al. 2014, for more discussion on seasonal biases), net precipitation, or information about moisture source rather than amount.

Our modeling experiments found an enhancement of the summer monsoon systems with increased summer insolation, as did numerous previous studies of past monsoons (e.g. Kutzbach and Otto-Bliesner 1982; Tuentner et al. 2003; Braconnot et al. 2008). This enhancement is also found in records from northern Africa and South America and shown in Fig. 1a by the anti-phasing of the north African humidity index of Tjallingii et al. (2008) and Gulf of Guinea sea surface salinity reconstruction of Weldeab et al. (2007) with the South American cave records of Wang et al. (2004, 2007), Cruz et al. (2005) and Bolivian salt flat sediment core of Fritz et al. (2004). The much-studied African Humid Period, during which grass and low shrub vegetation expanded northward into the Sahel-Sahara region, coincides with a maximum in NH summer insolation (Gasse 2000; DeMenocal et al. 2000). The precessional response of the north African summer monsoon is limited during MIS2 and 3, when eccentricity is low, and the high latitude ice sheets impact atmospheric circulation over northern Africa (Weldeab et al. 2007; Tjallingii et al. 2008; Timm et al. 2010; Kuechler et al. 2013). This can be seen in Fig. 1b, where the phase relationship between precipitation maxima and precession varies between precessional cycles.

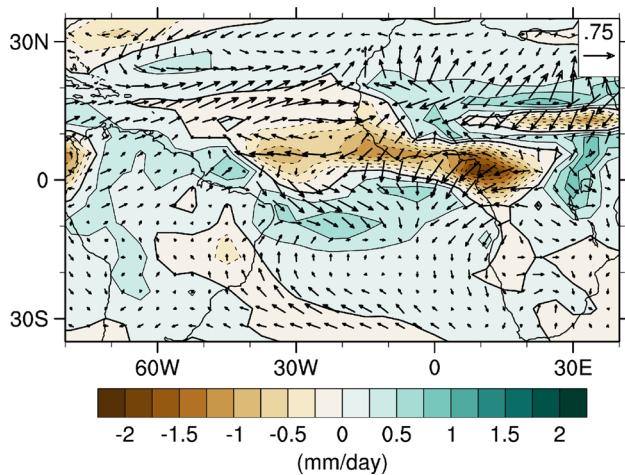


**Fig. 13** Eccentricity rectification of annual mean precipitation (mm/day; colors) and surface winds (m/s; vectors); see Eq. (10)

Reconstructions of oceanic precipitation, i.e. position and intensity of the Atlantic ITCZ, are scarce. Deplazes et al. (2013) argue that changes in sediment reflectance in Cariaco Basin 10°N are indicative of meridional ITCZ shifts. Their record mainly shows variability on millennial time-scales, while variability on precessional time-scales is limited; maximum precipitation is not in phase with maximum summer insolation (Fig. 1). In our modeling study, there is very little change in annual mean precipitation over Venezuela and the Cariaco Basin in response to precession (Fig. 4b), suggesting that precipitation over this area might have a different seasonal sensitivity to precession. Arbuszewski et al. (2013) inferred information about the timing and magnitude of meridional ITCZ shifts since the LGM from a compilation of terrestrial and marine paleorecords. They find that the ITCZ shifted southward during the LGM, and subsequently shifted northward during the Holocene. While the southward shift at the LGM was likely strongly influenced by high-latitude processes (see discussion above), the Holocene northward shift lends support to our finding that enhancement of the terrestrial summer monsoon over north Africa ( $P_{\text{MIN}}$ ) is accompanied by a northward shift of the ITCZ (Figs. 5, 7a). Unfortunately this reconstruction barely spans a precessional cycle, making it difficult to assess the consistency of the response to precessional forcing throughout the Pleistocene. To our knowledge there are no reconstructions of paleo-precipitation from the central tropical Atlantic that could be used for a more robust comparison with our modeling results over the ocean. The general agreement between our model simulations and paleo-reconstructions of tropical precipitation give confidence that our results are robust, in spite of Atlantic mean state biases common in GCMs (Sect. 2).

### 4.3 Eccentricity as a rectifier

As was noted before, the strength of the precessional cycle is strongly modulated by eccentricity: The influence of precession is strong for high values of eccentricity, while it would be non-existent if Earth's orbit were perfectly circular. In this study we therefore used a high value of eccentricity (0.067, the highest value over the past 51 Ma (Laskar et al. 2004)) to have the most pronounced signal.

The eccentricity cycle itself is only associated with a small change in annual mean insolation. Yet numerous records from the Pleistocene, Pliocene, and earlier times show substantial variability on eccentricity time scales, in particular its strongest periodicity, 400,000 years (e.g. Tiedemann et al. 1994; Herbert 1997; Tian et al. 2002; Wang et al. 2010). This variability must therefore come about through nonlinear rectification of the precessional cycle. A measure of this rectification is the degree to which the mean between maximum ( $P_{\text{MAX}}$ ) and minimum ( $P_{\text{MIN}}$ ) precession deviates from the zero eccentricity state ( $E_{\text{ZERO}}$ ):

$$x_{\text{rect}} = \frac{x_{P_{\text{MAX}}} + x_{P_{\text{MIN}}}}{2} - x_{E_{\text{ZERO}}} \quad (10)$$

This eccentricity rectification is shown for precipitation and surface winds in Fig. 13. The precipitation and wind changes shown in this figure are quite substantial. They amount to  $\sim 10 - 20\%$  of our modeled precessional changes (Figs. 7, 11).

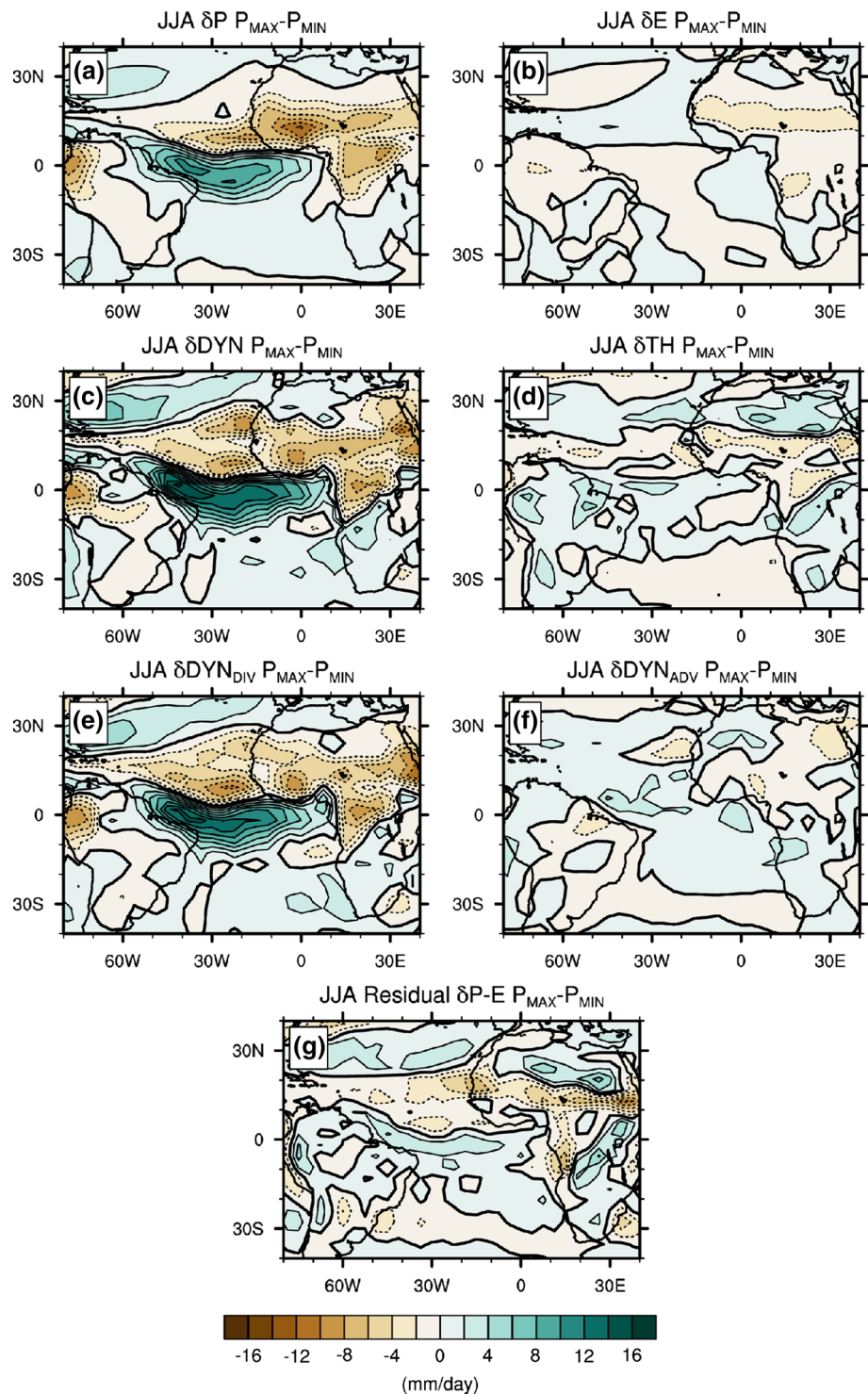
Eccentricity rectification over the continents is especially apparent over northern Africa, where there might be strong soil moisture and vegetation feedbacks rectifying the response, and equatorial Africa, suggesting interactions with the Atlantic cold tongue. Over the ocean, there is a meridional shift of the ITCZ that is associated with strong wind changes over the Atlantic and near the coast of Africa. These wind changes imply changes in upwelling and hence productivity changes that could be reflected in the  $\delta^{13}\text{C}$  records containing 400 ka eccentricity variability (Tiedemann et al. 1994; Herbert 1997; Tian et al. 2002; Wang et al. 2010).

## 5 Summary and conclusion

A simplified view of the response of tropical hydroclimate to precessional forcing is that precipitation increases with local summer insolation (Masson-Delmotte et al. 2013). Many previous modeling studies have therefore focused on the seasonal response of tropical precipitation to precession. Here we compare two idealized experiments with the earth system model CESM1.0.3 to address the mechanisms



**Fig. 14** JJA  $P_{\text{MAX}}-P_{\text{MIN}}$  change in precipitation (**a**); contributions to this change from changes in **b** evaporation; **c** winds ( $\delta\text{DYN}$  in Eq. (12)), **d** specific humidity ( $\delta\text{TH}$  in Eq. (12)), **e** divergence ( $\delta\text{DYN}_{\text{DIV}}$  in Eq. (13)) and **f** advection ( $\delta\text{DYN}_{\text{ADV}}$  in Eq. (13)); and **g** the difference between diagnosed and modeled changes in net precipitation

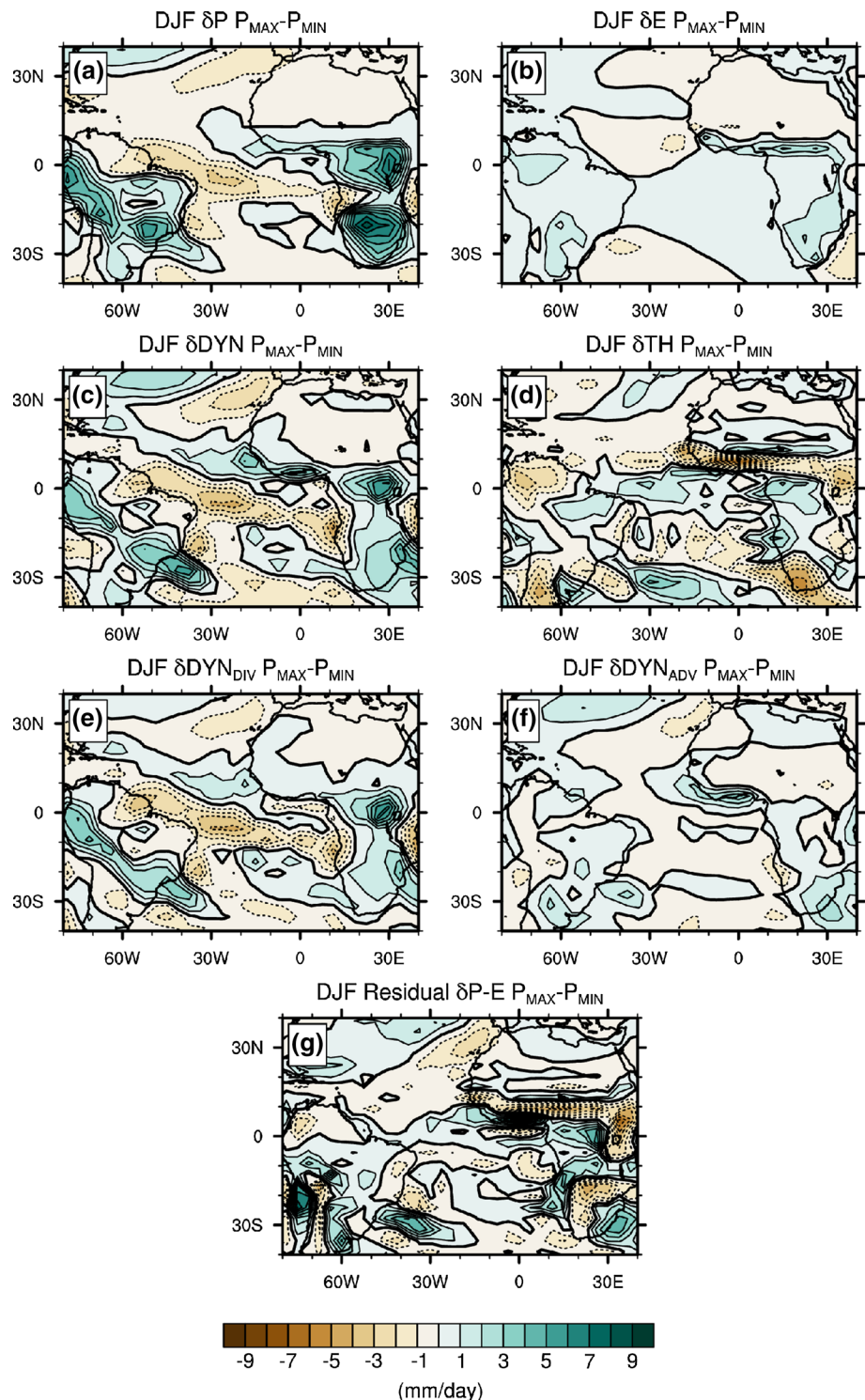


that rectify the *annual mean* precipitation response to precessional forcing. The model simulations are run with maximum precession  $P_{\text{MAX}}$  and minimum precession  $P_{\text{MIN}}$ ; eccentricity is set to 0.067 to maximize the response (see Table 1).

In the zonal annual mean, the tropical precipitation response follows the expected pattern of the warmer

summer hemisphere getting wetter (Fig. 4a). However, the regional characteristics of annual mean precipitation changes (Fig. 4b) are much more complex, especially over the oceans. This suggests that classical zonal mean frameworks of understanding the ITCZ are not able to explain regional changes. In our analysis we focus on the Atlantic Ocean, which displays a meridional dipole response in

**Fig. 15** DJF  $P_{\text{MAX}} - P_{\text{MIN}}$  change in precipitation (a); contributions to this change from changes in b evaporation; c winds ( $\delta\text{DYN}$  in Eq. (12)), d specific humidity ( $\delta\text{TH}$  in Eq. (12)), e divergence ( $\delta\text{DYN}_{\text{DIV}}$  in Eq. (13)) and f advection ( $\delta\text{DYN}_{\text{ADV}}$  in Eq. (13)); and g the difference between diagnosed and modeled changes in net precipitation



precipitation with its axis north of the equator. The dipole is asymmetric, with an annual mean ocean precipitation response that is stronger south of its axis than north of it. Although the annual mean precipitation response over the Atlantic seems to follow the paradigm of warmer summer hemisphere getting wetter, a closer examination of its phase reveals that this is not true on an instantaneous

basis. Figure 5c shows that Atlantic precipitation actually *decreases* in the season with more TOA insolation.

The simulated seasonal precipitation response mostly derives from changes in the mean circulation, in particular changes in atmospheric divergence (see “Appendix”). This is in contrast to the findings of Merlis et al. (2013), who in an aquaplanet simulation with slab ocean and fixed clouds

attributed a precessionally induced ITCZ shift to thermodynamic processes. Our results therefore show the importance of continents, dynamic ocean processes and cloud changes in driving the tropical precipitation response to precession. In our simulations, seasonal temperature and precipitation changes over the continents play a key role in driving precipitation changes over the Atlantic ocean (Fig. 6).

Temperature changes over northern Africa in boreal spring and summer (Fig. 7a) lead to wind changes over the North Atlantic (Fig. 7b), which through changes in the latent heat flux (Fig. 9d) set up an anomalous SST gradient (Fig. 8c) that affects the *position* of the ITCZ (Fig. 5c). This boundary layer mechanism is amplified by the WES-feedback (Fig. 9d) and changes in equatorial ocean heat transport (Fig. 9f). Under maximum precession, continental temperatures in boreal spring and summer decrease in response to a reduction in TOA insolation, strengthening the trades, reducing the meridional SST gradient, and keeping the ITCZ south. These processes are illustrated in the upper panel of Fig. 6. Similar mechanisms do not operate in boreal fall and winter, when TOA insolation forcing is stronger over the Southern Hemisphere (Fig. 2b). This is because continental temperatures over southern Africa show a weaker response to insolation forcing (compare Figs. 7a, 8, 9, 10, 11b) and oceanic winds are particularly sensitive to continental forcing over the North Atlantic (Chiang et al. 2001; Xie and Saito 2001). This asymmetric seasonal change in ITCZ position leads to an annual mean change in Atlantic ITCZ position.

Continental monsoon changes and their associated diabatic forcing alter the stability of the troposphere and impact the *intensity* of precipitation over the ocean. Figure 6 shows schematically how under maximum precession, precipitation over the African continent decreases in boreal spring and summer (Fig. 7b), increasing precipitation over the Atlantic ocean (Fig. 10). In boreal fall and winter,  $P_{\text{MAX}}$  precipitation over southern Africa and South America increases (Fig. 11b), leading to a reduction in oceanic precipitation (Fig. 12). Because the continental precipitation response to precessional forcing is stronger in JJA than in DJF (Table 2), the annual mean response is skewed towards this season. It should be noted that we are analyzing a strongly coupled system, which means that without additional sensitivity experiments we cannot conclusively prove our proposed path of causality. However, further diagnosis using the  $F_{\text{NET}}$  framework of Neelin and Held (1987) (not shown) supports the idea that changes in moisture convergence over the continent are a direct response to shortwave forcing, unlike oceanic precipitation changes which are indirectly forced.

Direct comparison of our modeling results with paleoproxies is precluded by the fact that there are no long proxy records representing oceanic precipitation over the Atlantic.

Reconstructions of continental precipitation over Africa and South America confirm our finding that continental precipitation follows the warmer summer hemisphere (Gasse 2000; DeMenocal et al. 2000; Fritz et al. 2004; Wang et al. 2004, 2007; Cruz et al. 2005; Weldeab et al. 2007; Tjallingii et al. 2008). A sediment record from Cariaco Basin (Deplazes et al. 2013) is interpreted as reflecting shifts in ITCZ, but these occur mostly on millennial timescales. In our model, Cariaco Basin is not very sensitive to the phases of precessional forcing compared here. A reconstruction of ITCZ position by Arbuszewski et al. (2013) suggests that the ITCZ shifted northward during the mid-Holocene, which would be in line with our findings. However, their reconstruction only goes back to the LGM, so further comparisons cannot be made. During MIS2 and 3, when precessional forcing was weak, and the climate system was in a glacial state with strong global cooling, high-latitude (millennial) forcing likely dominated over the local precessional response.

Our results show that while orbital TOA insolation forcing is the same at all longitudes, regional responses are strongly zonally asymmetric as a result of interactions between terrestrial processes, oceanic changes and remote influences. They illustrate the importance of considering the seasonality of climatic forcings, even when studying annual mean climate change.

**Acknowledgments** Our work was supported through the US National Science Foundation under Grant #1341311. We would like to thank Dr. Fei-Fei Jin for insightful discussion of the concept of zonal mean ITCZ.

## Appendix: Moisture budget analysis

Changes in precipitation can be the result of changes in thermodynamics (a change in specific humidity as a result of temperature changes), by changes in mean circulation (the advection and convergence of moisture), by changes in the transient eddy moisture convergence, or by changes in evaporation. One can quantify these different contributions by determining the individual components that comprise the moisture budget. A similar approach was taken e.g. by Clement et al. (2004) and Merlis et al. (2013) for the precessional cycle, and by e.g. Held and Soden (2006) and Seager et al. (2010) for present-day climate change. Here we follow the formalism of Seager et al. (2010); a complete derivation can be found in Trenberth and Guillemot (1995).

The full moisture budget equation is:

$$\rho_w g(P - E) = - \int_0^{p_s} \nabla \cdot (\bar{\mathbf{u}} \bar{q}) dp - \int_0^{p_s} \nabla \cdot (\mathbf{u}' q') dp - q_s \mathbf{u}_s \cdot \nabla p_s \quad (11)$$



where overbars indicate monthly means, primes indicate deviations from the monthly mean,  $\rho_w$  is the density of water,  $P - E$  is precipitation minus evaporation,  $p$  is pressure,  $\mathbf{u}$  are the horizontal wind velocities,  $q$  is specific humidity, and subscripts  $s$  indicate surface values. The first term on the right-hand side describes moisture convergence by the mean flow, while the second term represents that due to transient eddies. The last term on the right-hand side is a surface term which is generally found to be small.

The  $P_{\text{MAX}} - P_{\text{MIN}}$  difference in the moisture budget becomes:

$$\begin{aligned} \delta(P - E) = & -\frac{1}{\rho_w g} \left\{ \int_0^{p_s} \nabla \cdot (\delta \bar{\mathbf{u}} \bar{q}_{P_{\text{MIN}}}) dp \right. \\ & + \int_0^{p_s} \nabla \cdot (\bar{\mathbf{u}}_{P_{\text{MIN}}} \delta \bar{q}) dp \\ & + \int_0^{p_s} \nabla \cdot \delta(\bar{\mathbf{u}}' q') dp \\ & + \int_0^{p_s} \nabla \cdot (\delta \bar{\mathbf{u}} \delta \bar{q}) dp \\ & \left. + \delta(q_s \mathbf{u}_s \cdot \nabla p_s) \right\} \\ \delta P = & \delta \text{DYN} + \delta \text{TH} + \delta \text{TE} + \delta \text{NL} - \delta \text{S} + \delta E \quad (12) \end{aligned}$$

where  $\delta$  is the difference operator. The first term on the right-hand side represents changes in the moisture budget due to changes in the monthly mean circulation; we will refer to this term as the ‘dynamic’ contribution,  $\delta \text{DYN}$ . The second term is the contribution due to changes in the monthly mean specific humidity, which will be referred to as the ‘thermodynamic’ term  $\delta \text{TH}$ . The third, fourth, and fifth term represent the transient eddy contribution  $\delta \text{TE}$ , the nonlinear product of circulation and humidity changes  $\delta \text{NL}$ , and changes in the surface term  $\delta \text{S}$ , respectively. These are either found to be small ( $\delta \text{NL}$  and  $\delta \text{S}$ ) or cannot be estimated from our model output ( $\delta \text{TE}$ ).

We can further split the dynamical term  $\delta \text{DYN}$  into a part relating to the anomalous convergence of the mean specific humidity field, and a part relating to the anomalous advection of the mean specific humidity gradient:

$$\begin{aligned} \delta \text{DYN} = & -\int_0^{p_s} (\bar{q}_{P_{\text{MIN}}} \nabla \cdot \delta \bar{\mathbf{u}}) dp - \int_0^{p_s} (\delta \bar{\mathbf{u}} \cdot \nabla \bar{q}_{P_{\text{MIN}}}) dp \\ = & \delta \text{DYN}_{\text{DIV}} + \delta \text{DYN}_{\text{ADV}} \quad (13) \end{aligned}$$

These various components are shown for JJA in Fig. 14 and for DJF in Fig. 15. First of all, it should be noted that the DJF precipitation response is smaller than the JJA response, especially over the ocean, and is not a mirror image of the JJA response. In both seasons, over the Atlantic Ocean as well as over the continents, the dynamic component (Figs. 14c, 15c) strongly dominates the response. Evaporation changes (Figs. 14b, 15b) are small, and generally of the same sign as the dynamical term. In JJA, the thermodynamic term (Fig. 14d) too is small, and generally

of the same sign as the dynamic term, except over the most northern part of Africa, the North Atlantic, and equatorial South America. In DJF on the other hand, the thermodynamic component (Fig. 15d) is mostly opposite in sign to the dynamic changes. In JJA as well as DJF, the dynamic component is made up almost entirely of the  $\delta \text{DYN}_{\text{DIV}}$  term (compare Fig. 14e with f and Fig. 15e with f). Differences between the diagnosed and modeled changes in net precipitation (Figs. 14g, 15g) stem from our ignoring of the transient eddy term, as well as calculation errors due to interpolation and discretization (Seager et al. 2010).

**Open Access** This article is distributed under the terms of the Creative Commons Attribution 4.0 International License (<http://creativecommons.org/licenses/by/4.0/>), which permits unrestricted use, distribution, and reproduction in any medium, provided you give appropriate credit to the original author(s) and the source, provide a link to the Creative Commons license, and indicate if changes were made.

## References

- Arbuszewski JA, DeMenocal PB, Cléroux C, Bradtmiller L, Mix A (2013) Meridional shifts of the Atlantic intertropical convergence zone since the last glacial maximum. *Nat Geosci* 6(11):959–962. doi:10.1038/ngeo1961
- Berger AL (1978) Long-term variations of daily insolation and quaternary climatic changes. *J Atmos Sci* 35:2362–2367
- Biasutti M, Battisti DS, Sarachik ES (2004) Mechanisms controlling the annual cycle of precipitation in the tropical Atlantic sector in an atmospheric GCM. *J Clim* 17:4708–4723
- Biasutti M, Battisti DS, Sarachik ES (2005) Terrestrial influence on the annual cycle of the Atlantic ITCZ in an AGCM coupled to a slab ocean model. *J Clim* 18(1):211–228. doi:10.1175/JCLI3262.1
- Bosmans JHC, Drijfhout S, Tuentner E, Lourens LJ, Hilgen FJ, Weber SL (2012) Monsoonal response to mid-Holocene orbital forcing in a high resolution GCM. *Clim Past* 8(2):723–740. doi:10.5194/cp-8-723-2012
- Braconnot P, Marti O (2003) Impact of precession on monsoon characteristics from coupled ocean atmosphere experiments: changes in Indian monsoon and Indian ocean climatology. *Mar Geol* 201(1–3):23–34
- Braconnot P, Marti O, Jousaume S, Leclainche Y (2000) Ocean feedback in response to 6 kyr BP insolation. *J Clim* 13:1537–1553
- Braconnot P, Marzin C, Grégoire L, Mosquet E, Marti O (2008) Monsoon response to changes in Earth’s orbital parameters: comparisons between simulations of the Eemian and of the Holocene. *Clim Past* 4(4):281–294. doi:10.5194/cp-4-281-2008
- Broccoli AJ, Dahl KA, Stouffer RJ (2006) Response of the ITCZ to Northern Hemisphere cooling. *Geophys Res Lett* 33:1–4. doi:10.1029/2005GL024546
- Chiang JC, Bitz CM (2005) Influence of high latitude ice cover on the marine intertropical convergence zone. *Clim Dyn* 25(5):477–496. doi:10.1007/s00382-005-0040-5
- Chiang JC, Friedman AR (2012) Extratropical cooling, inter-hemispheric thermal gradients, and tropical climate change. *Annu Rev Earth Planet Sci* 40(1):383–412. doi:10.1146/annurev-earth-042711-105545
- Chiang JC, Kushnir Y, Giannini A (2002) Deconstructing Atlantic intertropical convergence zone variability: influence of the local

- cross-equatorial sea surface temperature gradient and remote forcing from the eastern equatorial Pacific. *J Geophys Res* 107(D1):4004. doi:[10.1029/2000JD000307](https://doi.org/10.1029/2000JD000307)
- Chiang JC, Biasutti M, Battisti DS (2003) Sensitivity of the Atlantic inter-tropical convergence zone to last glacial maximum boundary conditions. *Paleoceanography* 18(4):1–18. doi:[10.1029/2003PA000916](https://doi.org/10.1029/2003PA000916)
- Chiang JCH, Zebiak SE, Cane MA (2001) Relative roles of elevated heating and surface temperature gradients in driving anomalous surface winds over tropical oceans. *J Atmos Sci* 58:1371–1394
- Chikamoto Y, Timmermann A, Stevenson S, DiNezio P, Langford S (2015) Decadal predictability of soil water, vegetation, and wildfire frequency over North America. *Clim Dyn*. doi:[10.1007/s00382-015-2469-5](https://doi.org/10.1007/s00382-015-2469-5)
- Claussen M, Fohlmeister J, Ganopolski A, Brovkin V (2006) Vegetation dynamics amplifies precessional forcing. *Geophys Res Lett* 33(9):2–5. doi:[10.1029/2006GL026111](https://doi.org/10.1029/2006GL026111)
- Clement AC, Hall A, Broccoli AJ (2004) The importance of precessional signals in the tropical climate. *Clim Dyn* 22(4):327–341. doi:[10.1007/s00382-003-0375-8](https://doi.org/10.1007/s00382-003-0375-8)
- Cruz FW, Burns SJ, Karmann I, Sharp WD, Vuillen M, Cardoso AO, Ferrari JA, Silva Dias PL, Viana O Jr (2005) Insolation-driven changes in atmospheric circulation over the past 116,000 years in subtropical Brazil. *Nature* 434:63–66
- DeMenocal PB, Ortiz J, Guilderson T, Adkins J, Sarnthein M, Baker L, Yarusinsky M (2000) Abrupt onset and termination of the African Humid Period: rapid climate responses to gradual insolation forcing. *Quatern Sci Rev* 19:347–361
- Deplazes G, Lückge A, Peterson LC, Timmermann A, Hamann Y, Ka Hugen, Röhl U, Laj C, Ma Cane, Sigman DM, Haug GH (2013) Links between tropical rainfall and North Atlantic climate during the last glacial period. *Nat Geosci* 6(3):213–217. doi:[10.1038/ngeo1712](https://doi.org/10.1038/ngeo1712)
- Deser C, Tomas RA, Sun L (2015) The role of ocean–atmosphere coupling in the zonal mean atmospheric response to Arctic sea ice loss. *J Clim* 28:2168–2186. doi:[10.1175/JCLI-D-14-00325.1](https://doi.org/10.1175/JCLI-D-14-00325.1)
- Donohoe A, Marshall J, Ferreira D, Mcgee D, Sciences P (2013) The relationship between ITCZ location and cross-equatorial atmospheric heat transport : From the seasonal cycle to the last glacial maximum. *J Clim* 26(11):3597–3618. doi:[10.1175/JCLI-D-12-00467.1](https://doi.org/10.1175/JCLI-D-12-00467.1)
- Dykoski CA, Edwards RL, Cheng H, Yuan D, Cai Y, Zhang M, Lin Y, Qing J, An Z, Revenaugh JS (2005) A high-resolution, absolute-dated Holocene and deglacial Asian monsoon record from Dongge Cave, China. *Earth Planet Sci Lett* 233(1–2):71–86. doi:[10.1016/j.epsl.2005.01.036](https://doi.org/10.1016/j.epsl.2005.01.036)
- EPICA Community Members (2004) Eight glacial cycles from an Antarctic ice core. *Nature* 429(6992):623–628. doi:[10.1038/nature02599](https://doi.org/10.1038/nature02599)
- Fritz SC, Baker PA, Lowenstein TK, Seltzer GO, Rigsby CA, Dwyer GS, Tapia PM, Arnold KK, Ku TL, Luo S (2004) Hydrologic variation during the last 170,000 years in the southern hemisphere tropics of South America. *Quatern Res* 61(1):95–104. doi:[10.1016/j.yqres.2003.08.007](https://doi.org/10.1016/j.yqres.2003.08.007)
- Fučkar NS, Xie SPP, Farneti R, Maroon EA, Frierson DMW (2013) Influence of the extratropical ocean circulation on the intertropical convergence zone in an idealized coupled general circulation model. *J Clim* 26(13):4612–4629. doi:[10.1175/JCLI-D-12-00294.1](https://doi.org/10.1175/JCLI-D-12-00294.1)
- Gasse F (2000) Hydrological changes in the African tropics since the last glacial maximum. *Quatern Sci Rev* 19(1–5):189–211. doi:[10.1016/S0277-3791\(99\)00061-X](https://doi.org/10.1016/S0277-3791(99)00061-X)
- Gent PR, Danabasoglu G, Donner LJ, Holland MM, Hunke EC, Jayne SR, Lawrence DM, Neale RB, Rasch PJ, Vertenstein M, Worley PH, Yang ZL, Zhang M (2011) The community climate system model version 4. *J Clim* 24(19):4973–4991. doi:[10.1175/2011JCLI4083.1](https://doi.org/10.1175/2011JCLI4083.1)
- Gill AE (1980) Some simple solutions for heat-induced tropical circulation. *Q J R Meteorol Soc* 106(449):447–462
- Held IM, Soden BJ (2006) Robust responses of the hydrological cycle to global warming. *J Clim* 19(21):5686–5699. doi:[10.1175/JCLI3990.1](https://doi.org/10.1175/JCLI3990.1)
- Herbert TD (1997) A long marine history of carbon cycle modulation by orbital-climatic changes. *Proc Nat Acad Sci* 94(16):8362–9
- Hurrell JW, Holland MM, Gent PR, Ghan S, Kay JE, Kushner PJ, Lamarque JF, Large WG, Lawrence D, Lindsay K, Lipscomb WH, Long MC, Mahowald N, Marsh DR, Neale RB, Rasch P, Vavrus S, Vertenstein M, Bader D, Collins WD, Hack JJ, Kiehl J, Marshall S (2013) The community earth system model: a framework for collaborative research. *Bull Am Meteorol Soc* 94(9):1339–1360. doi:[10.1175/BAMS-D-12-00121.1](https://doi.org/10.1175/BAMS-D-12-00121.1)
- Huybers P, Wunsch C (2003) Rectification and precession signals in the climate system. *Geophys Res Lett* 30(19):1–4. doi:[10.1029/2003GL017875](https://doi.org/10.1029/2003GL017875)
- Kang SM, Held IM, Frierson DMW, Zhao M (2008) The response of the ITCZ to extratropical thermal forcing: idealized slab-ocean experiments with a GCM. *J Clim* 21(14):3521–3532. doi:[10.1175/2007JCLI2146.1](https://doi.org/10.1175/2007JCLI2146.1)
- Kang SM, Frierson DMW, Held IM (2009) The tropical response to extratropical thermal forcing in an idealized GCM: the importance of radiative feedbacks and convective parameterization. *J Atmos Sci* 66(9):2812–2827. doi:[10.1175/2009JAS2924.1](https://doi.org/10.1175/2009JAS2924.1)
- Kang SM, Held IM, Xie SP (2014) Contrasting the tropical responses to zonally asymmetric extratropical and tropical thermal forcing. *Clim Dyn* 42(7–8):2033–2043. doi:[10.1007/s00382-013-1863-0](https://doi.org/10.1007/s00382-013-1863-0)
- Khon VC, Park W, Latif M, Mokhov II, Schneider B (2010) Response of the hydrological cycle to orbital and greenhouse gas forcing. *Geophys Res Lett* 37(19):L19,705. doi:[10.1029/2010GL044377](https://doi.org/10.1029/2010GL044377)
- Khon VC, Park W, Latif M, Mokhov II, Schneider B (2012) Tropical circulation and hydrological cycle response to orbital forcing. *Geophys Res Lett* 39(15):L15,708. doi:[10.1029/2012GL052482](https://doi.org/10.1029/2012GL052482)
- Koenig SJ, DeConto RM, Pollard D (2011) Late Pliocene to Pleistocene sensitivity of the Greenland Ice Sheet in response to external forcing and internal feedbacks. *Clim Dyn* 37(5–6):1247–1268. doi:[10.1007/s00382-011-1050-0](https://doi.org/10.1007/s00382-011-1050-0)
- Krebs U, Timmermann A (2007) Tropical air-sea interactions accelerate the recovery of the Atlantic Meridional Overturning Circulation after a major shutdown. *J Clim* 20(19):4940–4956. doi:[10.1175/JCLI4296.1](https://doi.org/10.1175/JCLI4296.1)
- Kuechler R, SchefußE Beckmann B, Dupont L, Wefer G (2013) NW African hydrology and vegetation during the last glacial cycle reflected in plant-wax-specific hydrogen and carbon isotopes. *Quatern Sci Rev* 82:56–67. doi:[10.1016/j.quascirev.2013.10.013](https://doi.org/10.1016/j.quascirev.2013.10.013)
- Kutzbach JE, Guetter PJ (1986) The influence of changing orbital parameters and surface boundary conditions on climate simulations for the past 18000 years. *J Atmos Sci* 43(16):1726–1759
- Kutzbach JE, Liu Z (1997) Response of the African monsoon to orbital forcing and ocean feedbacks in the middle Holocene. *Science* 278(5337):440–443. doi:[10.1126/science.278.5337.440](https://doi.org/10.1126/science.278.5337.440)
- Kutzbach JE, Otto-Bliesner BL (1982) The sensitivity of the African-Asian monsoonal climate to orbital parameter changes for 9000 years B.P. in a low-resolution General Circulation Model. *J Atmos Sci* 39(6):1177–1188
- Kutzbach JE, Liu X, Liu Z, Chen G (2008) Simulation of the evolutionary response of global summer monsoons to orbital forcing over the past 280,000 years. *Clim Dyn* 30(6):567–579. doi:[10.1007/s00382-007-0308-z](https://doi.org/10.1007/s00382-007-0308-z)
- Laepple T, Lohmann G (2009) Seasonal cycle as template for climate variability on astronomical timescales. *Paleoceanography* 24(4):1–15. doi:[10.1029/2008PA001674](https://doi.org/10.1029/2008PA001674)
- Laepple T, Werner M, Lohmann G (2011) Synchronicity of Antarctic temperatures and local solar insolation on orbital timescales. *Nature* 471(7336):91–4. doi:[10.1038/nature09825](https://doi.org/10.1038/nature09825)

- Laskar J, Robutel P, Joutel F, Gastineau M, Correia ACM, Levrard B (2004) A long-term numerical solution for the insolation quantities of the Earth. *Astronomy Astrophys* 428(1):261–285. doi:[10.1051/0004-6361:20041335](https://doi.org/10.1051/0004-6361:20041335)
- Lindzen RS, Hou AY (1988) Hadley circulations for zonally averaged heating centered off the equator. *J Atmos Sci* 45(17):2416–2427
- Lindzen RS, Nigam S (1987) On the role of sea surface temperature gradients in forcing low-level winds and convergence in the Tropics. *J Atmos Sci* 44(17):2418–2436
- Marshall J, Kushnir Y, Battisti DS, Chang P, Czaja A, Dickson R, Hurrell J, McCartney M, Saravanan R, Visbeck M (2001) North Atlantic climate variability: phenomena, impacts and mechanisms. *Int J Climatol* 21(15):1863–1898. doi:[10.1002/joc.693](https://doi.org/10.1002/joc.693)
- Marshall J, Armour KC, Scott JR, Kostov Y, Hausmann U, Ferreira D, Shepherd TG, Bitz CM (2014) The ocean's role in polar climate change: asymmetric Arctic and Antarctic responses to greenhouse gas and ozone forcing. *Philos Trans R Soc A* 372(20130):040
- Marzin C, Braconnot P, Kageyama M (2013) Relative impacts of insolation changes, meltwater fluxes and ice sheets on African and Asian monsoons during the Holocene. *Clim Dyn*. doi:[10.1007/s00382-013-1948-9](https://doi.org/10.1007/s00382-013-1948-9)
- Masson-Delmotte V, Schulz M, Abe-Ouchi A, Beer J, Ganopolski A, Gonzalez Rouco JF, Jansen E, Lambeck K, Luterbacher J, Naish TR, Osborn T, Otto-Bliesner BL, Quinn T, Ramesh R, Rojas M, Shao X, Timmermann A (2013) Information from Paleoclimate Archives. In: Stocker TF, Qin D, Plattner GK, Tignor M, Allen SK, Boschung J, Nauels A, Xia Y, Bex V, Midgley PM (eds) *Climate change 2013: the physical science basis. Contribution of Working Group I to the Fifth Assessment Report of the Intergovernmental Panel on Climate Change*, Cambridge University Press, Cambridge, United Kingdom and New York, NY, USA, pp 383–464
- Menviel L, Timmermann A, Friedrich T, England MH (2014) Hindcasting the continuum of Dansgaard–Oeschger variability: mechanisms, patterns and timing. *Clim Past* 10(1):63–77. doi:[10.5194/cp-10-63-2014](https://doi.org/10.5194/cp-10-63-2014)
- Merlis TM, Schneider T, Bordoni S, Eisenman I (2013) The tropical precipitation response to orbital precession. *J Clim* 26(6):2010–2021. doi:[10.1175/JCLI-D-12-00186.1](https://doi.org/10.1175/JCLI-D-12-00186.1)
- Milankovitch M (1941) Kanon der Erdbestrahlung und seine Anwendung auf das Eiszeitenproblem. In: Royal Serbian Academy Special Publication 132, vol 33, Royal Serbian Academy, Belgrade, p 633
- Mitchell TP, Wallace JM (1992) The annual cycle in equatorial convection and sea surface temperature. *J Clim* 5:1140–1156
- Moore JK, Lindsay K, Doney SC, Long MC, Misumi K (2013) Marine ecosystem dynamics and biogeochemical cycling in the community earth system model [CESM1(BGC)]: comparison of the 1990s with the 2090s under the RCP4.5 and RCP8.5 scenarios. *J Clim* 26(23):9291–9312. doi:[10.1175/JCLI-D-12-00566.1](https://doi.org/10.1175/JCLI-D-12-00566.1)
- Neelin JD, Held IM (1987) Modeling tropical convergence based on the moist static energy budget. *Mon Weather Rev* 115(1):3–12
- Nobre P, Shukla J (1996) Variations of sea surface temperature, wind stress, and rainfall over the Tropical Atlantic and South America. *J Clim* 9:2464–2479
- North Greenland Ice Core Project Members (2004) High-resolution record of Northern Hemisphere climate extending into the last interglacial period. *Nature* 431:147–151. doi:[10.1038/nature02805](https://doi.org/10.1038/nature02805)
- Paillard D (2001) Glacial cycles: toward a new paradigm. *Rev Geophys* 39(3):325–346
- Rial JA, Pielke RA Sr, Beniston M, Claussen M, Canadell J, Cox P, Held H, de Noblet-Ducoudré N, Prinn R, Reynolds JF, Salas JD (2004) Nonlinearities, feedbacks and critical thresholds within the Earth's climate system. *Clim Change* 65:11–38
- Richter I, Xie SP, Wittenberg AT, Masumoto Y (2012) Tropical Atlantic biases and their relation to surface wind stress and terrestrial precipitation. *Clim Dyn* 38(5–6):985–1001. doi:[10.1007/s00382-011-1038-9](https://doi.org/10.1007/s00382-011-1038-9)
- Richter I, Xie SP, Behera SK, Doi T, Masumoto Y (2014) Equatorial Atlantic variability and its relation to mean state biases in CMIP5. *Clim Dyn* 42(1–2):171–188. doi:[10.1007/s00382-012-1624-5](https://doi.org/10.1007/s00382-012-1624-5)
- Schneider EK (1977) Axially symmetric steady-state models of the basic state for instability and climate studies. Part II. Nonlinear calculations. *J Atmos Sci* 34(2):280–296
- Schneider T, Bischoff T, Haug GH (2014) Migrations and dynamics of the intertropical convergence zone. *Nature* 513(7516):45–53. doi:[10.1038/nature13636](https://doi.org/10.1038/nature13636)
- Seager R, Naik N, Vecchi GA (2010) Thermodynamic and dynamic mechanisms for large-scale changes in the hydrological cycle in response to global warming. *J Clim* 23(17):4651–4668. doi:[10.1175/2010JCLI3655.1](https://doi.org/10.1175/2010JCLI3655.1)
- Shi Z, Liu XD, Sun Y, An Z, Liu Z, Kutzbach JE (2011) Distinct responses of East Asian summer and winter monsoons to astronomical forcing. *Clim Past* 7(4):1363–1370. doi:[10.5194/cp-7-1363-2011](https://doi.org/10.5194/cp-7-1363-2011)
- Shields CA, Bailey DA, Danabasoglu G, Jochum M, Kiehl JT, Levis S, Park S (2012) The low-resolution CCSM4. *J Clim* 25(12):3993–4014. doi:[10.1175/JCLI-D-11-00260.1](https://doi.org/10.1175/JCLI-D-11-00260.1)
- Siongco AC, Hohenegger C, Stevens B (2014) The Atlantic ITCZ bias in CMIP5 models. *Clim Dyn*. doi:[10.1007/s00382-014-2366-3](https://doi.org/10.1007/s00382-014-2366-3)
- Stevenson S, Timmermann A, Chikamoto Y, Langford S, DiNezio P (2015) Stochastically generated North American Megadroughts. *J Clim* 28(5):1865–1880. doi:[10.1175/JCLI-D-13-00689.1](https://doi.org/10.1175/JCLI-D-13-00689.1)
- Tachikawa K, Timmermann A, Vidal L, Sonzogni C, Timm OE (2014) CO<sub>2</sub> radiative forcing and intertropical convergence zone influences on western Pacific warm pool climate over the past 400 ka. *Quatern Sci Rev* 86:24–34. doi:[10.1016/j.quascirev.2013.12.018](https://doi.org/10.1016/j.quascirev.2013.12.018)
- Tian J, Wang P, Cheng X, Li Q (2002) Astronomically tuned Plio–Pleistocene benthic  $\delta^{18}\text{O}$  record from South China Sea and Atlantic-Pacific comparison. *Earth Planet Sci Lett* 203:1015–1029
- Tiedemann R, Sarnthein M, Shackleton NJ (1994) Astronomic timescale for the Pliocene Atlantic  $\delta^{18}\text{O}$  and dust flux records of Ocean Drilling Program site 659. *Paleoceanography* 9(4):619–638
- Timm OE, Köhler P, Timmermann A, Menviel L (2010) Mechanisms for the onset of the African Humid Period and Sahara Greening 14.5–11 ka BP. *J Clim* 23(10):2612–2633. doi:[10.1175/2010JCLI3217.1](https://doi.org/10.1175/2010JCLI3217.1)
- Timmermann A, Okumura Y, An SI, Clement AC, Dong B, Guilyardi E, Hu A, Jungclauss JH, Renold M, Stocker TF, Stouffer RJ, Sutton R, Xie SP, Yin JH (2007) The influence of a weakening of the Atlantic meridional overturning circulation on ENSO. *J Clim* 20(19):4899–4919. doi:[10.1175/JCLI4283.1](https://doi.org/10.1175/JCLI4283.1)
- Timmermann A, Friedrich T, Timm OE, Chikamoto MO, Abe-Ouchi A, Ganopolski A (2014) Modeling obliquity and CO<sub>2</sub> effects on Southern Hemisphere climate during the past 408 ka. *J Clim* 27(5):1863–1875. doi:[10.1175/JCLI-D-13-00311.1](https://doi.org/10.1175/JCLI-D-13-00311.1)
- Tjallingii R, Claussen M, Stuut JBW, Fohlmeister J, Jahn A, Bickert T, Lamy F, Röhl U (2008) Coherent high- and low-latitude control of the northwest African hydrological balance. *Nat Geosci* 1(10):670–675. doi:[10.1038/ngeo289](https://doi.org/10.1038/ngeo289)
- Tomas RA, Webster PJ (1997) The role of inertial instability in determining the location and strength of near-equatorial convection. *Q J R Meteorol Soc* 123(541):1445–1482
- Tomas RA, Holton JR, Webster PJ (1999) The influence of cross-equatorial pressure gradients on the location of near-equatorial convection. *Q J R Meteorol Soc* 125(556):1107–1127. doi:[10.1002/qj.1999.49712555603](https://doi.org/10.1002/qj.1999.49712555603)



- Trenberth KE, Guillemot CJ (1995) Evaluation of the global atmospheric moisture budget as seen from analyses. *J Clim* 8:2255–2272
- Tuenter E (2004) Modeling orbital induced variations in circum-Mediterranean climate. PhD thesis, Universiteit Utrecht
- Tuenter E, Weber SL, Hilgen FJ, Lourens LJ (2003) The response of the African summer monsoon to remote and local forcing due to precession and obliquity. *Glob Planet Change* 36(4):219–235
- Tuenter E, Weber SL, Hilgen FJ, Lourens LJ (2005) Sea-ice feedbacks on the climatic response to precession and obliquity forcing. *Geophys Res Lett* 32(24):2–5. doi:[10.1029/2005GL024122](https://doi.org/10.1029/2005GL024122)
- Wang P, Tian J, Lourens LJ (2010) Obscuring of long eccentricity cyclicity in Pleistocene oceanic carbon isotope records. *Earth Planet Sci Lett* 290(3–4):319–330. doi:[10.1016/j.epsl.2009.12.028](https://doi.org/10.1016/j.epsl.2009.12.028)
- Wang X, Auler AS, Edwards RL, Cheng H, Cristalli PS, Smart PL, Richards DA, Shen CC (2004) Wet periods in northeastern Brazil over the past 210 kyr linked to distant climate anomalies. *Nature* 432(7018):740–743. doi:[10.1038/nature03067](https://doi.org/10.1038/nature03067)
- Wang X, Auler AS, Edwards RL, Cheng H, Ito E, Wang Y, Kong X, Solheid M (2007) Millennial-scale precipitation changes in southern Brazil over the past 90,000 years. *Geophys Res Lett* 34(23):1–5. doi:[10.1029/2007GL031149](https://doi.org/10.1029/2007GL031149)
- Wang Y, Cheng H, Edwards RL, Kong X, Shao X, Chen S, Wu J, Jiang X, Wang X, An Z (2008) Millennial- and orbital-scale changes in the East Asian monsoon over the past 224,000 years. *Nature* 451(7182):1090–3. doi:[10.1038/nature06692](https://doi.org/10.1038/nature06692)
- Weldeab S, Lea DW, Schneider RR, Andersen N (2007) 155,000 years of West African monsoon and ocean thermal evolution. *Science* 316(5829):1303–7. doi:[10.1126/science.1140461](https://doi.org/10.1126/science.1140461)
- Wyrwoll KH, Liu Z, Chen G, Kutzbach JE, Liu X (2007) Sensitivity of the Australian summer monsoon to tilt and precession forcing. *Quatern Sci Rev* 26(25–28):3043–3057. doi:[10.1016/j.quascirev.2007.06.026](https://doi.org/10.1016/j.quascirev.2007.06.026)
- Xie P, Arkin PA (1997) Global precipitation: A 17-year monthly analysis based on gauge observations, satellite estimates, and numerical model outputs. *Bull Am Meteorol Soc* 78(11):2539–2558
- Xie SP (1996) Effects of seasonal solar forcing on latitudinal asymmetry of the ITCZ. *J Clim* 9:2945–2950
- Xie SP (2005) The shape of continents, air–sea interaction, and the rising branch of the Hadley circulation. In: Diaz HF, Bradley RS (eds) *The Hadley circulation: present, past and future*. Kluwer Academic Publishers, chap 4, pp 121–152
- Xie SP, Carton JA (2004) Tropical Atlantic variability: patterns, mechanisms, and impacts. In: Wang C, Xie SP, Carton JA (eds) *Earth's climate: the ocean–atmosphere interaction*. Geophysical Monograph, AGU, Washington D.C., pp 1–26
- Xie SP, Philander SGH (1994) A coupled ocean–atmosphere model of relevance to the ITCZ in the eastern Pacific. *Tellus* 46A:340–350
- Xie SP, Saito K (2001) Formation and variability of a northerly ITCZ in a hybrid coupled AGCM: continental forcing and oceanic–atmospheric feedback. *J Clim* 14:1262–1276
- Zhao Y, Braconnot P, Marti O, Harrison SP, Hewitt CD, Kitoh A, Liu Z, Mikolajewicz U, Otto-Bliesner BL, Weber SL (2005) A multi-model analysis of the role of the ocean on the African and Indian monsoon during the mid-Holocene. *Clim Dyn* 25(7–8):777–800. doi:[10.1007/s00382-005-0075-7](https://doi.org/10.1007/s00382-005-0075-7)